SIAM J. NUMER. ANAL.
Vol. 56, No. 3, pp. 1818–1847

ACCURACY OF WENO AND ADAPTIVE ORDER WENO RECONSTRUCTIONS FOR SOLVING CONSERVATION LAWS*

TODD ARBOGAST†, CHIEH-SEN HUANG‡, AND XIKAI ZHAO§

Abstract. In this paper, we analyze standard weighted essentially nonoscillatory (WENO) reconstructions and multilevel WENO reconstructions with adaptive order (WENO-AO) using both WENO-JS and WENO-Z weighting. We also present a new WENO-AO reconstruction. We give conditions under which the reconstructions achieve optimal order accuracy for both smooth solutions and solutions with discontinuities. The old WENO-AO reconstruction drops to a fixed, base level of approximation when there are discontinuities in the solution, but the new one maintains the accuracy of the largest stencil over which the solution is smooth. Our analysis in the discontinuous case requires that the smoothness indicators do *not* approach zero as the grid is refined. We provide a condition to ensure this result, but we also show an example where this can fail to occur. That is, we show that WENO reconstructions can fail to maintain the order of approximation of the smallest stencil over which the solution is smooth. We also present numerical results confirming the convergence theory of the old and new WENO-AO reconstructions and compare their performance in solving conservation laws.

Key words. weighted essentially nonoscillatory, WENO-AO, polynomial reconstruction, hyperbolic equation, approximation, shock discontinuity, contact discontinuity

AMS subject classifications. 65D05, 65M08, 65M06, 65M12, 76M12, 76M20

DOI. 10.1137/17M1154758

1. Introduction.

For solving a system of hyperbolic conservation laws,

$$u_t + f(u)_x = 0, \quad t > 0,\ x \in \mathbb{R},\ u \in \mathbb{R}^d,\ d \geq 1, \tag{1.1}$$

weighted essentially nonoscillatory (WENO) schemes [8, 14, 13] are a popular choice. They allow one to reconstruct a high order version of the solution merely from approximations of cell averages (in finite volume schemes) or point values (in finite difference schemes). The key is to average approximations defined on various stencils and to weight them so as to avoid stencils containing a discontinuity in the solution. The idea is that high order accuracy may be achieved by the approximation on the big stencil where the solution is smooth and yet reduce to the order of the smaller stencils when there is a shock or contact discontinuity to avoid.

It appears that standard WENO reconstructions were not proved to have this property until 2011, when Aràndiga et al. gave a proof [1]. They clarified the delicate nature of the parameters used in the standard nonlinear weighting procedure, WENO-JS, of Jiang and Shu [10]. The parameters are ϵ and η, where ϵ is a factor to avoid

*Received by the editors November 2, 2017; accepted for publication (in revised form) April 25, 2018; published electronically June 26, 2018.
http://www.siam.org/journals/sinum/56-3/M115475.html
Funding: This work was supported in part by U.S. National Science Foundation grant DMS-1418752, Taiwan Ministry of Science and Technology grant MOST 105-2115-M-110-006-MY2 through the Multidisciplinary and Data Science Research Center of the National Sun Yat-sen University, and the National Center for Theoretical Sciences, Taiwan.
†Institute for Computational Engineering and Sciences, University of Texas, Austin, TX 78712-1229 (arbogast@ices.utexas.edu).
‡Department of Applied Mathematics, National Sun Yat-sen University, Kaohsiung 804, Taiwan, Republic of China (huangcs@math.nsysu.edu.tw).
§Department of Mathematics, University of Texas, Austin, TX 78712-1202 (xzhao@math.utexas.edu).

division by zero and η is an exponent in the weight design (see (2.7)). In particular, ϵ needs to be proportional to h^2, where h is the the grid spacing, and $\eta > s/2$, where the low order polynomials approximate to order s. Kolb [11] later analyzed the CWENO3 scheme of Levy, Puppo, and Russo [12]. This latter paper provided a new way to obtain WENO reconstructions involving combining polynomials of different degrees, e.g., as done by Cravero et al. [5]. The idea was further generalized by Zhu and Qiu [16] and Balsara, Garain, and Shu [2] to define the class of multilevel WENO reconstructions with adaptive order (WENO-AO).

In this paper, we analyze the accuracy of the standard WENO and WENO-AO reconstructions. We include results for when the WENO-Z weighting procedure of Castro, Costa, and Don [4, 3, 6] is used. Our results are summarized in sections 4.3.5 and 5.3. The standard WENO reconstruction behaves as desired, even with WENO-Z weights [6]. It is high order accurate when the solution is smooth, and it drops to low order s when there is a discontinuity (not on the central cell), provided only that $\eta \geq s/2$. We show that this condition is sharp. The two-level WENO-AO(r, s) reconstructions behave similarly. They can achieve higher order r accuracy in the smooth case and otherwise maintain at least order s accuracy, provided that when using WENO-JS weights, $r \leq 2s - 1$ and $\eta \geq s/2$. WENO-Z weights are more complex, because the accuracy of the reconstruction depends more strongly on the choice of η, as we will show.

Multilevel WENO-AO$_s(r_\ell, \ldots, r_1, s)$ reconstructions [2] are based on a base state with approximation order s. When the solution is smooth the approximation attains the highest order r_ℓ, but when it is discontinuous, it usually drops to the base level s. When using WENO-JS weights, one requires $r_\ell \leq 2s - 1$ and $\eta \geq s/2$, which is equivalent to the two-level case. That is, from the point of view of approximation order, there is no point in using the multilevel reconstruction. Again, WENO-Z weights are more complex. There is a restriction on the size of the gap between successive approximation levels, but a careful choice of η can allow any order. However, the accuracy almost always drops to order s when the solution is discontinuous.

We present a new multilevel WENO-AO$(r_\ell, \ldots, r_1, r_0)$ reconstruction that has no base level. When the solution is smooth the approximation attains the highest order r_ℓ, but when it is discontinuous, it drops to the order of the largest stencil that does not contain the discontinuity.

When the solution has a discontinuity, our convergence results require the smoothness indicators $\sigma \nrightarrow 0$ as the grid is refined, as is the case in [1, 11, 5]. We show that this hypothesis can fail, and we replace it by the hypothesis that the discontinuity is bounded away from the gridpoints as the grid is refined (Definition 5.1). We further show that there are sequences of grids for which even this hypothesis fails. In that case, it is possible that a WENO reconstruction fails to maintain the lowest order of approximation. This seems contrary to the prevailing understanding of WENO reconstructions appearing in the literature.

The paper is structured as follows. In the next section, we give the background needed to understand WENO reconstruction techniques. For the knowledgable reader, this section, and the next, set our notation. In section 3, we define the various WENO reconstructions and define our new one. Section 4 presents a rigorous analysis of the errors in the reconstructions when the solution is smooth. We provide conditions needed to ensure that the reconstruction achieves the order of accuracy of the big stencil. In section 5, we give our analysis for the case when the solution has a discontinuity. Our cautionary example of a situation where a WENO reconstruction fails to maintain the lowest order of approximation appears in section 6. Finally, numerical results comparing the old and new WENO-AO reconstructions are given in the last section.

2. Background on WENO reconstructions.

We first review the background setting required for WENO reconstructions. For simplicity of exposition, we consider the finite volume framework. The finite difference reconstruction is similar.

Partition space by gridpoints $\cdots < x_{-1} < x_0 < x_1 < \cdots$. Define the cell $I_i = [x_i, x_{i+1}]$, its length $\Delta x_i = x_{i+1} - x_i$, and its midpoint $x_{i+\frac{1}{2}} = \frac{1}{2}(x_i + x_{i+1})$. Let $h = \max_i \Delta x_i$ and assume that the grid is quasi-uniform (i.e., there is some $\rho > 0$ such that $\rho h \le \min_i \Delta x_i$, so $\rho h \le \Delta x_i \le h$ for all i). Let $\bar{u}_i$ be the average of $u(x)$ on the cell I_i, i.e.,

$$\bar{u}_i = \frac{1}{\Delta x_i} \int_{I_i} u(x)\, dx. \tag{2.1}$$

2.1. Polynomial approximation on stencils.

Now assume that u is smooth. For an rth order approximation of u on a given cell I_i, we consider the ordered stencil $S_j^r(i)$, which contains r cells, including I_i, and is defined by

$$S_j^r(i) = \left\{ I_{i+j-\lfloor \frac{r}{2} \rfloor}, \dots, I_i, \dots, I_{i+j+\lfloor \frac{r-1}{2} \rfloor} \right\}, \tag{2.2}$$

where $-\left\lfloor \frac{r-1}{2} \right\rfloor \le j \le \left\lfloor \frac{r}{2} \right\rfloor$. Moreover, S_0^r denotes the central stencil. For the remainder of the paper, we fix a value of i and drop it from the notation. For each S_j^r, we obtain the rth order stencil polynomial P_j^r (a polynomial of degree $r-1$) by imposing the interpolation conditions

$$\frac{1}{\Delta x_k} \int_{I_k} P_j^r(x)\, dx = \bar{u}_k \quad \forall I_k \in S_j^r. \tag{2.3}$$

2.2. Smoothness indicators.

The smoothness indicator σ defined by Jiang and Shu in [10] is normally used to measure the smoothness of stencil polynomials on the cell I_i. For the stencil S_j^r, it is given by

$$\sigma_j^r = \sum_{\ell=1}^{r-1} \int_{I_i} (\Delta x_i)^{2\ell-1} \left(\frac{d^\ell P_j^r(x)}{dx^\ell} \right)^2 dx. \tag{2.4}$$

Since the grid is quasi-uniform, in regions where u is smooth, the Taylor expansion of (2.4) gives

$$\sigma_j^r = (u'h)^2 + \mathcal{O}(h^4), \tag{2.5}$$

which is $\mathcal{O}(h^2)$ or $\mathcal{O}(h^4)$ at a critical point. If there are discontinuities in u within the stencil S_j^r, then $\sigma_j^r = \mathcal{O}(1)$. It is not clear to the authors that a proof of this fact appears in the literature. One way to see it is to note that σ_j^r is a continuous function of $\bar{u}_k \in [-\|u\|_{L^\infty}, \|u\|_{L^\infty}]$ and $\Delta x_k / h \in [\rho, 1]$ for a finite set of k; that is, σ_j^r is a continuous function on a fixed, compact set as $h \to 0$ and so attains its maximum, which is therefore bounded. Summarizing,

$$\sigma_j^r = \begin{cases} \mathcal{O}(h^2) & \text{if } u \text{ is smooth on } S_j^r, \\ \mathcal{O}(1) & \text{if } u \text{ has a jump discontinuity on } S_j^r. \end{cases} \tag{2.6}$$

2.3. Nonlinear weights. A WENO reconstruction is a weighted sum of stencil polynomials. For the stencil S_j^r, let us denote its (constant) weight as α_j^r. We refer to this weight as a *linear* weight. For the linear weight α_j^r, we define its *nonlinear weight* $\tilde{\alpha}_j^r$, as discussed below.

For some collection of distinct stencils $S_{j_\ell}^{r_\ell}$, $\ell = 1, 2, \ldots, L$, we merely require that the linear weights sum to one, i.e., $\sum_\ell \alpha_{j_\ell}^{r_\ell} = 1$. (We also desire that $\alpha_{j_\ell}^{r_\ell} > 0$.) When the solution u is smooth, the linear weights should be chosen so as to give a high order WENO reconstruction. However, when there are discontinuities in the data over some stencils, we want to bias the weighted sum so as to exclude those stencils. The idea is to make $\tilde{\alpha}_{j_\ell}^{r_\ell} \simeq \alpha_{j_\ell}^{r_\ell}$ when u is smooth on $S_{j_\ell}^{r_\ell}$ and to make $\tilde{\alpha}_{j_\ell}^{r_\ell} \simeq 0$ when u is not smooth on $S_{j_\ell}^{r_\ell}$.

2.3.1. WENO-JS weights. For complete generality, let the linear weights be $\alpha_{j_\ell}^{r_\ell}$ for various ℓ. To define the nonlinear weights, Jiang and Shu [10] scale each linear weight $\alpha_{j_\ell}^{r_\ell}$ as

$$\hat{\alpha}_{j_\ell}^{r_\ell} = \frac{\alpha_{j_\ell}^{r_\ell}}{(\sigma_{j_\ell}^{r_\ell} + \epsilon_h)^\eta}, \tag{2.7}$$

and then normalize to define

$$\tilde{\alpha}_j^r = \tilde{\alpha}_{k_m}^{r_m} = \frac{\hat{\alpha}_{k_m}^{r_m}}{\sum_\ell \hat{\alpha}_{j_\ell}^{r_\ell}}, \tag{2.8}$$

for some exponent $\eta \geq 1$ and $\epsilon_h > 0$, which avoids any possibility of division by zero. Usually, one takes $\eta = 2$ and $\epsilon_h = \epsilon \simeq 10^{-6}$. Aràndiga et al. [1] show that, in fact, η must be chosen carefully and that it is valuable to take $\epsilon_h = Kh^2$ for some fixed $K > 0$. We will see this in sections 4–5.

2.3.2. WENO-Z weights. For standard WENO, Castro, Costa, and Don give the general formula for the WENO-Z reconstruction in [4] for $r \geq 3$. First let $m = \left\lfloor \frac{r}{2} \right\rfloor$ and use the smoothness indicators to define

$$\tau = \begin{cases} |\sigma_{-m}^r - \sigma_m^r| & \text{if } r \text{ is odd}, \\ |\sigma_{-m+1}^r - \sigma_{-m+2}^r - \sigma_{m-1}^r + \sigma_m^r| & \text{if } r \text{ is even}. \end{cases} \tag{2.9}$$

Then the unnormalized nonlinear weights are, for $\eta \geq 1$,

$$\hat{\alpha}_j^r = \alpha_j^r \left(1 + \left(\frac{\tau}{\sigma_j^r + \epsilon_h}\right)^\eta\right), \tag{2.10}$$

and the normalized weights are given by (2.8).

3. WENO reconstructions. In this section, we review the standard and adaptive order WENO reconstructions. We also present our new adaptive order WENO reconstruction. Within the notation for the reconstructions, we use r or $r_\ell, r_{\ell-1}, \ldots, r_1$ to denote the size of the bigger stencils and s or $s = r_0$ to denote the size of the smallest stencils.

3.1. Standard WENO reconstruction. Suppose we are interested in an $r = (2s-1)$st order standard WENO reconstruction for $s \geq 2$. First consider all the small stencils with s cells containing the given cell I_i. For each S_j^s, we construct P_j^s. Moreover, we define the big stencil $S_0^r = \bigcup_j S_j^s$ and construct a higher order polynomial P_0^r on it. At a fixed point x^*, the polynomial P_0^r can often be written as a convex combination of P_j^s, so

$$P_0^r(x^*) = \sum_j \alpha_j^s P_j^s(x^*), \tag{3.1}$$

where $\sum_j \alpha_j^s = 1$. We refer to α_j^s as an *exact* linear weight. These weights can be precomputed for the given x^* (if they do indeed exist).

When there are discontinuities in the data over the big stencil S_0^r, we want to make use of the relatively small stencils on which u is smooth in order to achieve the essentially nonoscillatory property. The standard WENO reconstruction, valid only for $x = x^*$, is

$$R_r(x^*) = \sum_j \tilde{\alpha}_j^s P_j^s(x^*). \tag{3.2}$$

3.2. WENO reconstructions with adaptive order (WENO-AO). In [12], Levy, Puppo, and Russo describe a third order compact, central WENO scheme (CWENO). They use a somewhat different WENO reconstruction than the standard one (3.2), because the linear weights in (3.1) fail to exist when $r = 2$ $(2r - 1 = 3)$ and $x^* = x_{i+\frac{1}{2}}$. For the given cell I_i, they combine the *optimal* quadratic polynomial P_0^3 and two linear polynomials P_0^2 and P_1^2. Three advantages of their approach are that exact linear weights are not required, the weights can be taken to be positive, and the reconstruction holds for any point $x \in I_i$. The disadvantage is that the big stencil polynomial must be computed. Cravero et al. [5] generalized the approach to any order.

Zhu and Qiu describe a fifth order WENO reconstruction in [16], where they combined the fifth order stencil polynomial with two linear stencil polynomials. Later, Balsara, Garain, and Shu introduced a new class of WENO reconstructions with adaptive order in [2], which we will briefly recall below. The idea is to combine the three quadratic stencil polynomials with some higher order stencil polynomials.

3.2.1. Two-level WENO-AO reconstruction. The fifth order reconstruction WENO-AO(5,3) is based on the large stencil $S_0^5 = \{I_{i-2}, I_{i-1}, I_i, I_{i+1}, I_{i+2}\}$ and the three small stencils $S_{-1}^3 = \{I_{i-2}, I_{i-1}, I_i\}$, $S_0^3 = \{I_{i-1}, I_i, I_{i+1}\}$, $S_1^3 = \{I_i, I_{i+1}, I_{i+2}\}$, from which we obtain the stencil polynomials P_0^5, P_{-1}^3, P_0^3, and, P_1^3, respectively. The reconstruction is given by

$$R^{5,3}(x) = \frac{\tilde{\alpha}_0^5}{\alpha_0^5}\Big[P_0^5(x) - \sum_{j=-1}^{1} \alpha_j^3 P_j^3(x)\Big] + \sum_{j=-1}^{1} \tilde{\alpha}_j^3 P_j^3(x), \tag{3.3}$$

where α_0^5 and $\alpha_j^3,\ j = -1, 0, 1$, are arbitrary positive linear weights such that $\alpha_0^5 + \sum_j \alpha_j^3 = 1$. The linear weights can literally be chosen arbitrarily, subject only to positivity and sum constraints. The specific choice will have some subtle effect on the value of the reconstruction but not on its order of accuracy. In practice, one often takes the weights to be on the order of 1 and takes a somewhat larger weight for the big stencil.

Using the same idea, WENO-AO(7,3) is defined on the big stencil S_0^7 and the same small stencils S_{-1}^3, S_0^3, S_1^3, and WENO-AO(9,3) is given on S_0^9, S_{-1}^3, S_0^3, S_1^3. In analogy with (3.3), the general formulation of WENO-AO(r,s) reconstruction,

$r > s \geq 2$, can be written as

$$R^{r,s}(x) = R_s^{r,s}(x) = \frac{\tilde{\alpha}_0^r}{\alpha_0^r}\Big[P_0^r(x) - \sum_j \alpha_j^s P_j^s(x)\Big] + \sum_j \tilde{\alpha}_j^s P_j^s(x), \tag{3.4}$$

where $S_0^r \supseteq \cup_j S_j^s \neq \emptyset$. The positive linear weights α_0^r and α_j^s can be chosen arbitrarily up to requiring $\alpha_0^r + \sum \alpha_j^s = 1$. If WENO-Z weights are used, following [2], the definition of τ is generalized to

$$\tau = \frac{1}{|\#\text{ of } j|} \sum_j |\sigma_0^r - \sigma_j^s|. \tag{3.5}$$

We remark that in [5], the smoothness indicator σ_0^r is based on the modified polynomial $\frac{1}{\alpha_0^r}\big[P_0^r(x) - \sum_j \alpha_j^s P_j^s(x)\big]$. This minor difference does not seem to matter much in either the theory or the computations.

3.2.2. Multilevel WENO-AO$_s$ reconstruction. It is possible that the solution on S_0^7 is nonsmooth but S_0^5 gives a smooth solution, so Balsara, Garain, and Shu [2] combine $R_3^{7,3}$ and $R_3^{5,3}$. The algorithm is given by

$$R_3^{7,5,3}(x) = \frac{\tilde{\gamma}^{7,3}}{\gamma^{7,3}}\big[R_3^{7,3}(x) - \gamma^{5,3} R_3^{5,3}(x)\big] + \tilde{\gamma}^{5,3} R_3^{5,3}(x), \tag{3.6}$$

where $\gamma^{7,3} + \gamma^{5,3} = 1$ and $\gamma^{7,3} > 0$, $\gamma^{5,3} > 0$ are arbitrary, and the nonlinear weighting is given below in (3.8)–(3.9).

Similarly, WENO-AO$_3$(9,5,3) is defined by $R_3^{9,3}$ and $R_3^{5,3}$. Using this recursive process WENO-AO$_3$(9,7,5,3) combines $R_3^{9,3}$ and $R_3^{7,5,3}$ [2], where each reconstruction includes the base order 3 polynomials. The generalized recursion formula of multilevel WENO-AO$_s(r_\ell, r_{\ell-1}, \ldots, r_1, s)$, $\ell \geq 1$, for approximation levels $r_\ell > r_{\ell-1} > \cdots > r_1 > s \geq 2$ and base level s, is (3.4) for $R_s^{r_k,s}(x)$ for all $1 \leq k \leq \ell$ and

$$\begin{aligned} R_s^{r_\ell, r_{\ell-1},\ldots,r_1,s}(x) = &\frac{\tilde{\gamma}^{r_\ell,s}}{\gamma^{r_\ell,s}}\big[R_s^{r_\ell,s}(x) - \gamma^{r_{\ell-1},\ldots,r_1,s} R_s^{r_{\ell-1},\ldots,r_1,s}(x)\big] \\ &+ \tilde{\gamma}_s^{r_{\ell-1},\ldots,r_1,s} R_s^{r_{\ell-1},\ldots,r_1,s}(x), \quad \ell \geq 2, \end{aligned} \tag{3.7}$$

where $S_0^{r_\ell} \supset S_0^{r_{\ell-1}} \supset \cdots \supset S_0^{r_1} \supseteq \cup_j S_j^s \neq \emptyset$. We could further generalize (3.7) to include all pertinent stencils, i.e., all $S_j^{r_m} \subset S_0^{r_\ell}$, but we omit the details.

The linear weights $\gamma^{r_\ell,s} > 0$ and $\gamma^{r_{\ell-1},\ldots,r_1,s} > 0$ are arbitrary such that $\gamma^{r_\ell,s} + \gamma^{r_{\ell-1},\ldots,r_1,s} = 1$. We define the WENO-JS nonlinear weights through the unnormalized weighting

$$\hat{\gamma}^{r_\ell,s} = \frac{\gamma^{r_\ell,s}}{(\sigma_0^{r_\ell} + \epsilon_h)^\eta}, \quad \hat{\gamma}^{r_{\ell-1},\ldots,r_1,s} = \frac{\gamma^{r_{\ell-1},\ldots,r_1,s}}{(\sigma_0^{r_{\ell-1}} + \epsilon_h)^\eta}, \tag{3.8}$$

and the normalized nonlinear weights are then

$$\tilde{\gamma}^{r_\ell,s} = \frac{\hat{\gamma}^{r_\ell,s}}{\hat{\gamma}^{r_\ell,s} + \hat{\gamma}^{r_{\ell-1},\ldots,r_1,s}}, \quad \tilde{\gamma}^{r_{\ell-1},\ldots,r_1,s} = \frac{\hat{\gamma}^{r_{\ell-1},\ldots,r_1,s}}{\hat{\gamma}^{r_\ell,s} + \hat{\gamma}^{r_{\ell-1},\ldots,r_1,s}} = 1 - \tilde{\gamma}^{r_\ell,s}. \tag{3.9}$$

For WENO-Z weights, when $\ell \geq 2$, define

$$\tau = |\sigma_0^{r_\ell} - \sigma_0^{r_{\ell-1}}|, \tag{3.10}$$

the unnormalized weights

$$\begin{aligned}\hat{\gamma}^{r_\ell,s} &= \gamma^{r_\ell,s}\Big(1+\Big(\frac{\tau}{\sigma_0^{r_\ell}+\epsilon_h}\Big)^{\eta}\Big),\\ \hat{\gamma}^{r_{\ell-1},\dots,r_1,s} &= \gamma^{r_{\ell-1},\dots,r_1,s}\Big(1+\Big(\frac{\tau}{\sigma_0^{r_{\ell-1}}+\epsilon_h}\Big)^{\eta}\Big),\end{aligned} \tag{3.11}$$

and the normalized nonlinear weights by (3.9). Note that $\sigma_0^{r_\ell}$ and $\sigma_0^{r_\ell-1}$ from the larger stencils are used in (3.8) and (3.11).

We can certainly use different values of η at each stage of the reconstruction. We will find this useful for the WENO-Z weights. In this case, we use $\eta_{0,k}$ in the initial stage (3.4) for $R_s^{r_k,s}(x)$, and we use η_ℓ in (3.11).

3.2.3. A new multilevel WENO-AO reconstruction. The original multilevel WENO-AO$_s$ reconstructions $R_s^{r_\ell,r_{\ell-1},\dots,r_1,s}$ in (3.7) are based on $R_s^{r_k,s}$, $1\le k\le \ell$; that is, at each level, the reconstructions may revert back to the base level s. As we will see, for each k, when u is smooth on $S_0^{r_k}$, r_k and s need to satisfy Theorem 4.4 below to have order r_k accuracy. Moreover, when u has a discontinuity on the two biggest stencils, Theorem 5.7 below shows that the order of accuracy is at best the base level s. Our goal is to define a new reconstruction that has no base level and thereby has relaxed constraints on the levels needed for accuracy and achieves a higher order of accuracy near discontinuities.

Define R^{r_1,r_0} as in (3.4), which uses the stencils $S_0^{r_1}$ and $S_j^{r_0}$ for several j. The new multilevel WENO-AO reconstruction has no base level, and it is denoted $R^{r_\ell,r_{\ell-1},\dots,r_0}$, where $r_\ell > r_{\ell-1} > \cdots > r_0 \ge 2$. It is given recursively for $\ell\ge 2$ by

$$\begin{aligned}R^{r_\ell,r_{\ell-1},\dots,r_0}(x) &= \frac{\tilde{\alpha}_0^{r_\ell}}{\alpha_0^{r_\ell}}\Big[P_0^{r_\ell}(x)-\Big(\sum_j \alpha_j^{r_0}\Big)R^{r_{\ell-1},\dots,r_0}(x)\Big]\\ &\quad+\Big(\sum_j \tilde{\alpha}_j^{r_0}\Big)R^{r_{\ell-1},\dots,r_0}(x),\end{aligned} \tag{3.12}$$

where $S_0^{r_\ell}\supset S_0^{r_{\ell-1}}\supset\cdots\supset S_0^{r_1}\supseteq \cup_j S_j^s\ne\emptyset$. Again, we could generalize this to include all pertinent stencils, but we do not pursue this here. The linear weights $\alpha_0^{r_\ell}>0$ and $\alpha_j^{r_0}>0$, for all j, are arbitrary such that $\alpha_0^{r_\ell}+\sum_j\alpha_j^{r_0}=1$. For WENO-Z weights, we define τ by (3.10). Compared to (3.7), note that here we use $P_0^{r_\ell}$ instead of R^{r_ℓ,r_0} and we use the smoothness indicators σ^{r_ℓ} and $\sigma_j^{r_0}$ for the nonlinear weighting. For example, the new multilevel WENO-AO(7,5,3) is defined as

$$R^{7,5,3}(x)=\frac{\tilde{\alpha}_0^{7}}{\alpha_0^{7}}\Big[P_0^{7}(x)-\Big(\sum_{j=-1}^{1}\alpha_j^{3}\Big)R^{5,3}(x)\Big]+\Big(\sum_{j=-1}^{1}\tilde{\alpha}_j^{3}\Big)R^{5,3}(x), \tag{3.13}$$

where $\tilde{\alpha}_0^7+\sum_j\tilde{\alpha}_j^3=1$ and $R^{5,3}(x)$ is given by (3.3).

4. Accuracy analysis when u is smooth. In this section, we give a rigorous analysis of the accuracy of WENO reconstructions in the case where u is smooth on the large stencil. We show under what conditions they give the desired accuracy. Our results can be viewed as generalizations of those in [1], where the authors analyzed standard WENO reconstructions, in [11], where the author proved the accuracy for the compact CWENO3 scheme and its reconstruction, and in [5], where two-level WENO reconstructions were analyzed. All three papers considered only WENO-JS weights. WENO-Z weights are considered in [6] for finite difference WENO.

At times, we require a tight assessment of asymptotic behavior. Recall that for a function $f(h)$,

$$f = \mathcal{O}(h^r) \quad \iff \quad |h^{-r} f| \le C \quad \text{as} \quad h \to 0 \tag{4.1}$$

for some constant $C > 0$. The notation $f = \Theta(h)$ provides upper and lower bounds:

$$f = \Theta(h^r) \quad \iff \quad C_1 h^r \le |f| \le C_2 h^r \quad \text{as} \quad h \to 0 \tag{4.2}$$

for some positive constants C_1 and C_2. In this notation, quasi uniformity of the grid means that $\Delta x_i = \Theta(h)$ for all i.

4.1. Smoothness indicators. We begin by looking at the smoothness indicators. The following lemma appears in [1] when comparing smoothness indicators on the same size stencils. When the stencil sizes differ, we have the result of Kolb [11], which deals only with the compact CWENO3 reconstruction, and [5]. We provide a simple proof that covers all cases.

LEMMA 4.1. *Let cell I_i and any stencils $S^r \ni I_i$ and $S^s \ni I_i$ be given (actually S^r_j and S^s_k, but the offsets j and k are immaterial). For $r \ge s \ge 2$, assume P^r and P^s are stencil polynomials from S^r and S^s, respectively. If the smoothness indicators σ^s and σ^r are given by* (2.4)*, then*

$$\sigma^r - \sigma^s = \mathcal{O}(h^{s+1}), \tag{4.3}$$

provided that u is smooth on $S^r \cup S^s$.

Proof. First we have that, for any $\ell = 0, 1, \ldots,$

$$\frac{d^\ell}{dx^\ell}\big(P^r - P^s\big) = \frac{d^\ell}{dx^\ell}\big(P^r - u\big) - \frac{d^\ell}{dx^\ell}\big(P^s - u\big) = \mathcal{O}(h^{\max(0,s-\ell)}). \tag{4.4}$$

Since

$$\begin{aligned}
\Big(\frac{d^\ell}{dx^\ell}P^r\Big)^2 &= \Big(\frac{d^\ell}{dx^\ell}P^s + \frac{d^\ell}{dx^\ell}(P^r - P^s)\Big)^2 \\
&= \Big(\frac{d^\ell}{dx^\ell}P^s\Big)^2 + \Big(\frac{d^\ell}{dx^\ell}(P^r - P^s)\Big)^2 + 2\frac{d^\ell}{dx^\ell}P^s\frac{d^\ell}{dx^\ell}(P^r - P^s),
\end{aligned}$$

we have that

$$\begin{aligned}
\sigma^r - \sigma^s &= \sum_{\ell=1}^{r-1} \Delta x_i^{2\ell-1} \int_{I_i} \Big[\Big(\frac{d^\ell}{dx^\ell}P^r\Big)^2 - \Big(\frac{d^\ell}{dx^\ell}P^s\Big)^2\Big]\,dx \\
&= \sum_{\ell=1}^{r-1} \Delta x_i^{2\ell-1} \int_{I_i} \Big[\Big(\frac{d^\ell}{dx^\ell}(P^r - P^s)\Big)^2 + 2\frac{d^\ell}{dx^\ell}P^s\frac{d^\ell}{dx^\ell}(P^r - P^s)\Big]\,dx \\
&= \sum_{\ell=1}^{r-1} \Delta x_i^{2\ell-1} \int_{I_i} \Big[\mathcal{O}(h^{\max(0,s-\ell)})^2 + 2\,\mathcal{O}(1)\,\mathcal{O}(h^{\max(0,s-\ell)})\Big]\,dx \\
&= \mathcal{O}(h^{s+1}).
\end{aligned}$$

∎

4.2. Nonlinear weights. The following theorem quantifies the perturbation of the nonlinear weights from the linear ones.

THEOREM 4.2. *Let $\eta \geq 1$, $\epsilon > 0$, and $K > 0$. Let cell I_i and $\ell \geq 1$ be given. For a collection of $\ell+1$ stencils $S^{r_k} \ni I_i$, $k = 0, 1, \dots, \ell$, where $2 \leq r_0 \leq r_1 \leq \cdots \leq r_\ell$, let α^{r_k} be positive linear weights such that $\sum_k \alpha^{r_k} = 1$, and let σ^{r_k} be the corresponding smoothness indicators. If u is smooth on $\bigcup_{k=0}^{\ell} S^{r_k}$, then the following hold:*

1. *WENO-JS weights satisfy, for all $k = 0, 1, \dots, \ell$,*

$$\tilde{\alpha}^{r_k} = \alpha^{r_k} + \begin{cases} \mathcal{O}(h^{r_0+1}) & \text{if } \epsilon_h = \epsilon, \\ \mathcal{O}(h^{r_0-1}) & \text{if } \epsilon_h = Kh^2. \end{cases} \tag{4.5}$$

2. *WENO-Z weights satisfy, for all $k = 0, 1, \dots, \ell$,*

$$\tilde{\alpha}^{r_k} = \alpha^{r_k} + \begin{cases} \mathcal{O}(h^{r_0+1+(r_m+1)\eta}) & \text{if } \epsilon_h = \epsilon, \\ \mathcal{O}(h^{r_0-1+(r_m-1)\eta}) & \text{if } \epsilon_h = Kh^2, \end{cases} \tag{4.6}$$

where $\tau = |\sigma^{r_\ell} - \sigma^{r_m}| = \mathcal{O}(h^{r_m+1})$ for some $0 \leq m \leq \ell$.

Proof. We first prove the results for the WENO-JS weights. For any k, we have

$$\tilde{\alpha}^{r_k} = \frac{\dfrac{\alpha^{r_k}}{(\sigma^{r_k}+\epsilon_h)^\eta}}{\displaystyle\sum_{j=0}^{\ell} \frac{\alpha^{r_j}}{(\sigma^{r_j}+\epsilon_h)^\eta}} = \frac{\alpha^{r_k}}{\displaystyle\sum_{j=0}^{\ell} \alpha^{r_j} \frac{(\sigma^{r_k}+\epsilon_h)^\eta}{(\sigma^{r_j}+\epsilon_h)^\eta}} = \frac{\alpha^{r_k}}{\displaystyle\sum_{j=0}^{\ell} \alpha^{r_j} \Big(1 + \frac{\sigma^{r_k}-\sigma^{r_j}}{\sigma^{r_j}+\epsilon_h}\Big)^\eta}. \tag{4.7}$$

Now by (2.6),

$$\sigma^{r_j} + \epsilon_h = \begin{cases} \Theta(1) & \text{if } \epsilon_h = \epsilon, \\ \Theta(h^2) & \text{if } \epsilon_h = Kh^2, \end{cases} \tag{4.8}$$

and by Lemma 4.1, we have

$$\sigma^{r_k} - \sigma^{r_j} = \mathcal{O}(h^{\min(r_k, r_j)+1}). \tag{4.9}$$

Hence

$$\sum_{j=0}^{\ell} \alpha^{r_j} \Big(1 + \frac{\sigma^{r_k}-\sigma^{r_j}}{\sigma^{r_j}+\epsilon_h}\Big)^\eta = \begin{cases} 1 + \mathcal{O}(h^{r_0+1}) & \text{if } \epsilon_h = \epsilon, \\ 1 + \mathcal{O}(h^{r_0-1}) & \text{if } \epsilon_h = Kh^2. \end{cases} \tag{4.10}$$

Combining this with (4.7) and recalling that $r_0 \geq 2$ shows that the result (4.5) holds for the WENO-JS weights.

Now for the WENO-Z weights, let $\rho_{r_j} = \tau/(\sigma^{r_j} + \epsilon_h)$ and write

$$\tilde{\alpha}^{r_k} = \frac{\alpha^{r_k}(1+\rho_{r_k}^\eta)}{\sum_j \alpha^{r_j}(1+\rho_{r_j}^\eta)} = \frac{\alpha^{r_k}(1+\rho_{r_k}^\eta)}{1 + \sum_j \alpha^{r_j} \rho_{r_j}^\eta}. \tag{4.11}$$

For any j, since $\tau = |\sigma^{r_\ell} - \sigma^{r_m}| = \mathcal{O}(h^{r_m+1})$,

$$\rho_{r_j} = \frac{\tau}{\sigma^{r_j}+\epsilon_h} = \begin{cases} \mathcal{O}(h^{r_m+1}) & \text{if } \epsilon_h = \epsilon, \\ \mathcal{O}(h^{r_m-1}) & \text{if } \epsilon_h = Kh^2, \end{cases} \tag{4.12}$$

by (4.8)–(4.9). Since $r_0 \geq 2$, $\rho_{r_j} \to 0$ as $h \to 0$, and so

$$\begin{aligned}\tilde{\alpha}^{r_k} &\sim \alpha^{r_k}(1+\rho_{r_k}^{\eta})\Big(1-\sum_j \alpha^{r_j}\rho_{r_j}^{\eta}\Big)\\ &\sim \alpha^{r_k}\Big(1+\rho_{r_k}^{\eta}-\sum_j \alpha^{r_j}\rho_{r_j}^{\eta}\Big)\\ &= \alpha^{r_k}\Big(1+\sum_j \alpha^{r_j}(\rho_{r_k}^{\eta}-\rho_{r_j}^{\eta})\Big).\end{aligned} \tag{4.13}$$

The mean value theorem shows that

$$\rho_{r_k}^{\eta}-\rho_{r_j}^{\eta} = \eta\,\xi^{\eta-1}\,(\rho_{r_k}-\rho_{r_j}) \tag{4.14}$$

for some ξ between ρ_{r_k} and ρ_{r_j}. Furthermore, by (4.8)–(4.9) and (4.12), for all k and j,

$$\begin{aligned}\rho_{r_k}-\rho_{r_j} &= \tau\Big(\frac{1}{\sigma^{r_k}+\epsilon_h}-\frac{1}{\sigma^{r_j}+\epsilon_h}\Big)\\ &= \tau\frac{\sigma^{r_k}-\sigma^{r_j}}{(\sigma^{r_k}+\epsilon_h)(\sigma^{r_j}+\epsilon_h)}\\ &= \begin{cases}\mathcal{O}(h^{r_m+r_0+2}) & \text{if } \epsilon_h=\epsilon,\\ \mathcal{O}(h^{r_m+r_0-2}) & \text{if } \epsilon_h=Kh^2.\end{cases}\end{aligned} \tag{4.15}$$

Combining (4.12)–(4.15) gives the conclusion (4.6). ◻

4.3. Accuracy. We now present our results on the accuracy of the various WENO reconstructions when u is smooth. After this presentation, we provide a discussion of the results.

4.3.1. Standard WENO. For standard WENO, we generalize the results in [1, 6] as follows.

THEOREM 4.3. *Let $\eta \geq 1$, $\epsilon > 0$, and $K > 0$. When u is smooth on S_0^r, $r = 2s-1$, $s \geq 2$, the standard WENO reconstruction $R_r(x)$ is order r accurate at the point x^* defined in* (3.2)*, using $\epsilon_h = \epsilon$ or Kh^2 and either WENO-JS or WENO-Z weights.*

Proof. We consider only the case of WENO-Z weights, since the case of WENO-JS weights is similar and can be found in [1]. By Lemma 4.1, $\tau = \mathcal{O}(h^{s+1})$, so (4.6) is valid. We compute that

$$\begin{aligned}R_r(x^*)-u(x^*) &= \sum_j \tilde{\alpha}_j^s(P_j^s(x^*)-u(x^*))\\ &= \sum_j \alpha_j^s(P_j^s(x^*)-u(x^*)) + \sum_j(\tilde{\alpha}_j^s-\alpha_j^s)(P_j^s(x^*)-u(x^*))\\ &= (P_0^r(x^*)-u(x^*)) + \sum_j(\tilde{\alpha}_j^s-\alpha_j^s)(P_j^s(x^*)-u(x^*))\\ &= \mathcal{O}(h^r)+\mathcal{O}(h^{(s-1)(\eta+1)})\mathcal{O}(h^s),\end{aligned} \tag{4.16}$$

using (4.6) with $r_j = r_m = r_0 = s$. ◻

4.3.2. WENO-AO(r,s). The next theorem gives the accuracy of convergence of two-level WENO-AO(r,s) given in (3.4).

THEOREM 4.4. *Let $\eta \geq 1$, $\epsilon > 0$, and $K > 0$. For $r > s \geq 2$, WENO-AO(r,s) has order of accuracy* $\min(r, r_{\max})$ *on I_i if u is smooth on S_0^r, where for WENO-JS weights,*

$$r_{\max} = \begin{cases} 2s+1 & \text{if } \epsilon_h = \epsilon, \\ 2s-1 & \text{if } \epsilon_h = Kh^2, \end{cases} \tag{4.17}$$

and for WENO-Z weights,

$$r_{\max} = r_{\max}(\eta) = \begin{cases} 2s+1+(s+1)\eta & \text{if } \epsilon_h = \epsilon, \\ 2s-1+(s-1)\eta & \text{if } \epsilon_h = Kh^2. \end{cases} \tag{4.18}$$

Proof. Because $\alpha_0^r + \sum_j \alpha_j^s = \tilde{\alpha}_0^r + \sum_j \tilde{\alpha}_j^s = 1$, we have on I_i that

$$\begin{aligned} R^{r,s} - u &= \frac{\tilde{\alpha}_0^r}{\alpha_0^r}\Big[(P_0^r - u) - \sum_j \alpha_j^s (P_j^s - u)\Big] + \sum_j \tilde{\alpha}_j^s (P_j^s - u) \\ &= \frac{\tilde{\alpha}_0^r}{\alpha_0^r}(P_0^r - u) - \sum_j \Big[\frac{\tilde{\alpha}_0^r - \alpha_0^r}{\alpha_0^r}\alpha_j^s - (\tilde{\alpha}_j^s - \alpha_j^s)\Big](P_j^s - u) \\ &= \mathcal{O}(h^r) + \sum_j \big[\mathcal{O}(\tilde{\alpha}_0^r - \alpha_0^r) + \mathcal{O}(\tilde{\alpha}_j^s - \alpha_j^s)\big]\mathcal{O}(h^s). \end{aligned} \tag{4.19}$$

Applying Theorem 4.2, we determine the value of $r_{\max}$. ∎

4.3.3. WENO-AO$_s(r_\ell, r_{\ell-1}, \ldots, r_1, s)$. We can extend the above theorem to the multilevel WENO-AO$_s(r_\ell, r_{\ell-1}, \ldots, r_1, s)$ given in (3.7).

THEOREM 4.5. *Let $\eta \geq 1$, $\epsilon > 0$, $K > 0$, and $\ell \geq 1$. Let $r_\ell > r_{\ell-1} > \cdots > r_1 > s \geq 2$, and assume that u is smooth on $S_0^{r_\ell}$. Then WENO-AO$_s(r_\ell, \ldots, r_1, s)$ has order of accuracy* $\min(r_\ell, r_{\max})$ *on I_i, where $r_{\max}$ is given by* (4.17) *for WENO-JS weights and* (4.18) *for WENO-Z weights when using a constant value for η.*

Moreover, if WENO-Z weights are used with variable η (i.e., $\eta_{0,k}$ is used in the initial stage (3.4) *for $R_s^{r_k,s}(x)$ and η_ℓ is used in* (3.11)*), then the reconstruction WENO-AO$_s(r_\ell, \ldots, r_1, s)$ has order of accuracy r_ℓ on I_i, provided that*

$$r_k \leq r_{\max}(\eta_{0,k}) \quad \forall 1 \leq k \leq \ell, \tag{4.20}$$

and, for all $2 \leq k \leq \ell$,

$$r_k \leq \begin{cases} s+1+r_{k-1}+(r_{k-1}+1)\eta_k & \text{if } \epsilon_h = \epsilon, \\ s-1+r_{k-1}+(r_{k-1}-1)\eta_k & \text{if } \epsilon_h = Kh^2, \end{cases} \tag{4.21}$$

$$r_k \leq \begin{cases} 3s+2+(r_{k-1}+1)\eta_k+(s+1)\eta_{\ell-1} & \text{if } \epsilon_h = \epsilon, \\ 3s-2+(r_{k-1}-1)\eta_k+(s-1)\eta_{\ell-1} & \text{if } \epsilon_h = Kh^2, \end{cases} \tag{4.22}$$

where $r_0 = s$ and $\eta_1 = \eta_{0,1}$.

Proof. For fixed $s \geq 2$, the proof proceeds by induction on $\ell \geq 1$. The result holds for $\ell = 1$ by Theorem 4.4. Assume the result holds for $\ell - 1 \geq 1$. We write the argument for variable η, since we can simply fix the value for the first part of the theorem. We compute on I_i that

$$
\begin{aligned}
&R_s^{r_\ell,r_{\ell-1},\dots,r_1,s} - u \\
&\quad= \frac{\tilde\gamma^{r_\ell,s}}{\gamma^{r_\ell,s}}\big[(R^{r_\ell,s}-u) - \gamma^{r_{\ell-1},\dots,r_1,s}(R^{r_{\ell-1},\dots,r_1,s}-u)\big] \\
&\qquad+ \tilde\gamma^{r_{\ell-1},\dots,r_1,s}(R^{r_{\ell-1},\dots,r_1,s}-u) \\
&\quad= \frac{\tilde\gamma^{r_\ell,s}}{\gamma^{r_\ell,s}}\big(R^{r_\ell,s}-u\big) - \Big[\frac{\tilde\gamma^{r_\ell,s}-\gamma^{r_\ell,s}}{\gamma^{r_\ell,s}}\gamma^{r_{\ell-1},\dots,r_1,s} \\
&\qquad\qquad - \big(\tilde\gamma^{r_{\ell-1},\dots,r_1,s} - \gamma^{r_{\ell-1},\dots,r_1,s}\big)\Big](R^{r_{\ell-1},\dots,r_1,s}-u) \\
&\quad= \mathcal{O}(h^{\min(r_\ell, r_{\max}(\eta_{0,\ell}))}) + \big[\mathcal{O}(\tilde\gamma^{r_\ell,s}-\gamma^{r_\ell,s}) \\
&\qquad\qquad + \mathcal{O}(\tilde\gamma^{r_{\ell-1},\dots,r_1,s}-\gamma^{r_{\ell-1},\dots,r_1,s})\big]\mathcal{O}(h^{\min(r_{\ell-1}, r_{\max}(\eta_\ell - 1))}),
\end{aligned} \tag{4.23}
$$

using Theorem 4.4 and induction. The linear and nonlinear weights sum to one, so $\tilde\gamma^{r_{\ell-1},\dots,r_1,s} - \gamma^{r_{\ell-1},\dots,r_1,s} = \gamma^{r_\ell,s} - \tilde\gamma^{r_\ell,s}$. If this perturbation of the linear weights is written as $\mathcal{O}(h^{w_\ell})$, then we have

$$
R_s^{r_\ell,r_{\ell-1},\dots,r_1,s} - u = \mathcal{O}\big(h^{\min(r_\ell, r_{\max}(\eta_{0,\ell}), w_\ell + r_{\ell-1}, w_\ell + r_{\max}(\eta_{\ell-1}))}\big), \tag{4.24}
$$

where w_ℓ is given in Theorem 4.2 with $r_m = r_{\ell-1}$, $r_0 = s$, and $\eta = \eta_\ell$ as

$$
w_\ell = \begin{cases} s \pm 1 & \text{for WENO-JS weights,} \\ s \pm 1 + (r_{\ell-1} \pm 1)\eta_\ell & \text{for WENO-Z weights,} \end{cases}
$$

respectively, for $\epsilon_h = \epsilon$ (+ sign) and $\epsilon_h = Kh^2$ (− sign).

For the first part of the theorem, WENO-Z weights use a constant η, and so both types of weights lead to $w_\ell + r_{\ell-1} \ge w_\ell + s \ge r_{\max}(\eta)$. Thus,

$$
\min(r_\ell, r_{\max}(\eta), w_\ell + r_{\ell-1}, w_\ell + r_{\max}(\eta)) = \min(r_\ell, r_{\max}(\eta)).
$$

For the second part of the theorem, i.e., when WENO-Z weights are used with variable η, note that

$$
w_\ell + r_{\ell-1} = s \pm 1 + (r_{\ell-1} \pm 1)\eta_\ell + r_{\ell-1} \ge r_\ell
$$

by (4.21). Moreover, (4.22) shows that

$$
w_\ell + r_{\max}(\eta_{\ell-1}) = 3s \pm 2 + (r_{\ell-1} \pm 1)\eta_\ell + (s \pm 1)\eta_{\ell-1} \ge r_\ell,
$$

so, with (4.20)

$$
\min(r_\ell, r_{\max}(\eta_{0,\ell}), w_\ell + r_{\ell-1}, w_\ell + r_{\max}(\eta_{\ell-1})) = r_\ell,
$$

and the proof is complete. ∎

4.3.4. WENO-AO($r_\ell, r_{\ell-1}, \dots, r_0$). The following theorem discusses the new reconstruction (3.12).

THEOREM 4.6. *Let $\epsilon > 0$, $K > 0$, and $\ell \ge 1$. Let $r_\ell > r_{\ell-1} > \cdots > r_0 \ge 2$, and assume that u is smooth on $S_0^{r_\ell}$. Let WENO-JS weights or WENO-Z weights be used with parameter $\eta_k \ge 1$ on level r_k, and define $r_{\max,0} = r_0$ and, for $1 \le k \le \ell$,*

$$
r_{\max,k} = \min(r_{k-1}, r_{\max,k-1}) + \begin{cases} r_0 \pm 1 & \textit{for WENO-JS weights,} \\ (r_0 \pm 1)(\eta_k + 1) & \textit{for WENO-Z weights,} \end{cases} \tag{4.25}
$$

respectively, for $\epsilon_h = \epsilon$ (+ sign) and $\epsilon_h = Kh^2$ (− sign). Then WENO-AO($r_\ell, \dots, r_0$) has order of accuracy $\min(r_\ell, r_{\max,\ell})$ *on I_i.*

Moreover, WENO-AO($r_\ell, \dots, r_0$) has order of accuracy r_ℓ on I_i if, for all $1 \le k \le \ell$,

$$r_k \le \begin{cases} r_{k-1} + r_0 \pm 1 & \textit{for WENO-JS weights,} \\ r_{k-1} + (r_0 \pm 1)(\eta_k + 1) & \textit{for WENO-Z weights.} \end{cases} \tag{4.26}$$

Proof. The proof is similar to the inductive proof of Theorem 4.5. The result holds for $\ell = 1$ by Theorem 4.4, so assume the result holds for $\ell - 1$. We compute on I_i that

$$\begin{aligned} &R^{r_\ell,\dots,r_0} - u \\ &\quad = \frac{\tilde\alpha_0^{r_\ell}}{\alpha_0^{r_\ell}}\Big[(P_0^{r_\ell} - u) - \Big(\sum_j \alpha_j^{r_0}\Big)(R^{r_{\ell-1},\dots,r_0} - u)\Big] + \Big(\sum_j \tilde\alpha_j^{r_0}\Big)(R^{r_{\ell-1},\dots,r_0} - u) \\ &\quad = \frac{\tilde\alpha_0^{r_\ell}}{\alpha_0^{r_\ell}}(P_0^{r_\ell} - u) - \Big[\frac{\tilde\alpha_0^{r_\ell} - \alpha_0^{r_\ell}}{\alpha_0^{r_\ell}}\Big(\sum_j \alpha_j^{r_0}\Big) - \sum_j(\tilde\alpha_j^{r_0} - \alpha_j^{r_0})\Big](R^{r_{\ell-1},\dots,r_0} - u). \end{aligned} \tag{4.27}$$

By Theorem 4.4 and induction, we have

$$R^{r_\ell,\dots,r_0} - u = \mathcal{O}(h^{r_\ell}) + \Big[\mathcal{O}(\tilde\alpha_0^{r_\ell} - \alpha_0^{r_\ell}) + \sum_j \mathcal{O}(\tilde\alpha_j^{r_0} - \alpha_j^{r_0})\Big]\mathcal{O}(h^{\min(r_{\ell-1}, r_{\max,\ell-1})}).$$

The perturbation of nonlinear weights is given by Theorem 4.2 with $r_m = r_0$, and the main result follows. The result (4.26) is given by requiring $r_k \le r_{\max,k}$ for all k. ◻

4.3.5. Discussion. Standard WENO reconstructions have a simple convergence theory. They give the optimal high order convergence rate whenever u is smooth.

The two-level WENO-AO(r, s) achieves the optimal convergence $\mathcal{O}(h^r)$ when the base level s is sufficiently high. In terms of the gap $r - s$ between levels, one needs

$$r - s \le \begin{cases} s \pm 1 & \text{for WENO-JS weights,} \\ (s \pm 1)(\eta + 1) & \text{for WENO-Z weights,} \end{cases} \tag{4.28}$$

respectively, for $\epsilon_h = \epsilon$ (+ sign) and $\epsilon_h = Kh^2$ (− sign). The WENO-Z weights are interesting in that one can adjust the value of η to reduce the constraint.

For the multilevel WENO reconstructions with adaptive order, the weights used have a marked effect on the results. The WENO-JS weights have a simple convergence theory. The optimal convergence $\mathcal{O}(h^{r_\ell})$ is attained by WENO-AO$_s(r_\ell, \dots, r_1, s)$ with base level s when

$$r_\ell - s \le s \pm 1, \tag{4.29}$$

but the new WENO-AO$(r_\ell, \dots, r_1, r_0)$ requires only that

$$r_k - r_{k-1} \le r_0 \pm 1 \quad \forall\, 1 \le k \le \ell. \tag{4.30}$$

The condition for WENO-AO$_s$ is that the largest gap $r_\ell - s$ must be bounded by $s \pm 1$, independent of the intermediate levels. In contrast, the new WENO-AO merely requires that each intermediate gap be bounded by this number, i.e., $r_0 \pm 1$.

Obtaining optimal accuracy with WENO-Z weights is a much more complex proposition. WENO-AO$_s(r_\ell,\dots,r_1,s)$ has the three conditions (4.20)–(4.22). The first condition is

$$r_k - s \le (s \pm 1)(\eta_{0,k}+1) \quad \forall\, 1 \le k \le \ell. \tag{4.31}$$

That is, each two-level approximation must be accurate, and then the gaps in the levels must satisfy the two relatively relaxed bounds (4.21)–(4.22). The new WENO-AO$(r_\ell,\dots,r_1,r_0)$ has only the condition (4.26), i.e.,

$$r_k - r_{k-1} \le (r_0 \pm 1)(\eta_k \pm 1) \quad \forall\, 1 \le k \le \ell. \tag{4.32}$$

This condition is worse than (4.21)–(4.22), but the very stringent condition (4.31) is removed.

A careful choice of η's can recover the full accuracy when using WENO-Z weights for any chosen approximation levels. As (4.32) shows, the new WENO-AO can use a bounded set of η's, whatever value for r_ℓ is taken. The condition (4.31) for WENO-AO$_s$ requires very large values of η when r_ℓ is taken very large.

While large values of η improve the convergence rates, they do so by strongly biasing the values of the nonlinear weights to that of the linear ones. This has a tendency to diminish the essentially nonoscillatory property of WENO schemes for solving problems with shocks and contact discontinuities. This was noticed in [2]: the authors remarked that WENO-JS weights were more stable, while WENO-Z weights gave better convergence results in the smooth case.

5. Accuracy analysis in the discontinuous case. We now consider the case when u is not smooth over the big stencil, but u is smooth on some of the smaller stencils. We consider only the case that u is smooth on a stencil or has a jump discontinuity somewhere in its interior. That is, we do not consider the intermediate case where u is continuous but pertinent derivatives are discontinuous, nor the case of multiple discontinuities, because we are interested in reconstructions involving a single shock or contact discontinuity.

5.1. Smoothness indicators in the discontinuous case. In general, when there is an actual discontinuity, it is true that the smoothness indicator is $\mathcal{O}(1)$, as noted in (2.6). However, it is far from obvious that $\sigma = \Theta(1)$, and this is in general not true, as we will see in Example 5.3 below. The result $\sigma = \Theta(1)$ holds for some particular sequences of grids.

DEFINITION 5.1. *Let $h>0$ and x_n^h be the gridpoints with maximal spacing h. For x_* fixed, let m be defined so $x_m^h \le x_* < x_{m+1}^h$. We say that x_* is* bounded away from the gridpoints *as $h \to 0$ if there exists a constant $c_* \in (0,1)$ such that*

$$0 < c_*\Delta x_m \le x_* - x_m^h \quad \textit{and} \quad 0 < c_*\Delta x_m \le x_{m+1}^h - x_*$$

for all h. We also say that the grids are bounded away from x_* *as $h \to 0$.*

LEMMA 5.2. *Let cell I_i and the stencil $S^r \ni I_i$, where $r \ge 2$, be given. Assume that u is smooth except for a jump discontinuity at $x_* \in I_m \in S^r$. If x_* is bounded away from the gridpoints as $h \to 0$, then the smoothness indicator*

$$\sigma^r = \Theta(1) \quad \textit{as} \quad h \to 0. \tag{5.1}$$

Proof. As noted after (2.5), σ^r is a continuous function of $\bar{u}_k \in [-\|u\|_{L^\infty}, \|u\|_{L^\infty}]$ and $\Delta x_k/h \in [\rho, 1]$ for a finite set of k. Therefore σ^r attains its finite maximum and its minimum on the fixed, compact set $[-\|u\|_{L^\infty}, \|u\|_{L^\infty}]^r \times [\rho, 1]^r$ as $h \to 0$, where ρ is the quasi-uniformity constant for the grid. The minimum value of $\sigma^r > 0$ for each fixed h, and the claim is that it remains strictly positive as $h \to 0$.

As $h \to 0$, if $\sigma^r \to 0$, then all the derivatives of P^r converge to 0 near I_i, i.e., P^r converges to some constant. However, as $h \to 0$,

$$\bar{u}_j = \mathcal{O}(h) + \begin{cases} u(x_*^-) & \text{if } j < m, \\ c(h) & \text{if } j = m, \\ u(x_*^+) & \text{if } j > m, \end{cases} \tag{5.2}$$

where $c(h)$ is between $c_* u(x_*^-) + (1 - c_*)\, u(x_*^+)$ and $(1 - c_*)\, u(x_*^-) + c_* u(x_*^+)$. Since $r \geq 2$, the lim-inf of the cell averages converge to at least two distinct values. So P^r cannot converge to a constant, which is a contradiction. Thus there exists some positive constant C such that $\sigma^r \geq C > 0$. ◻

We remark that for a specific stencil (actually a specific sequence of stencils), the proof shows that the smoothness indicator $\sigma^r \to 0$ only if x_* is near the endpoints of the stencil. That is, x_* must be in the leftmost or rightmost cell of the stencil. This is the only case in which as $h \to 0$, if we allowed $c_* \to 0$, then we would have only a single value for the cell averages arising in (5.2). However, WENO reconstruction involves a combination of substencils. So if the discontinuity is near the gridpoints anywhere in the big stencil, some small substencil will have this endpoint property. We thus make Definition 5.1 apply to all the gridpoints.

The above lemma does not hold for all sequences of grids, as shown in the next example, where $c_* = h$.

Example 5.3. Given cell $I_i = [h - h^2, 2h - h^2]$ and

$$u(x) = H(-x) = \begin{cases} 1, & x \leq 0, \\ 0, & x > 0, \end{cases} \tag{5.3}$$

where H is the Heaviside function, consider the stencil $S_0^2 = \{[-h^2, h - h^2], I_i\}$, for which the average of u on each cell is h and 0, respectively. The stencil polynomial is

$$P_0^2(x) = \frac{3h}{2} - h^2 - x,$$

and the smoothness indicator (2.4) is

$$\sigma_0^2 = h^2 = \Theta(h^2) \neq \Theta(1).$$

The literature is fraught with the belief that $\sigma \nrightarrow 0$ as $h \to 0$ when there is a discontinuity (e.g., in [1], this is assumed as a hypothesis, and in [11, 5], this belief is stated as being obvious).

5.2. WENO approximation on grids bounded away from the discontinuity. In [1], the authors showed that in the discontinuous case when the smoothness indicator $\sigma \nrightarrow 0$, WENO approximations are expected to converge only if $\epsilon_h = o(h)$, so we only consider the case $\epsilon_h = Kh^2$, $K > 0$ in this section. The next theorem gives the magnitude of WENO weights as $h \to 0$. The results for WENO-JS weights appear in [1] for standard WENO and in [11, 5] for two-level WENO-AO.

THEOREM 5.4. *Let $\eta \geq 1$, $K > 0$, and $\epsilon_h = Kh^2$. Given cell I_i, let $S^{r_j} \ni I_i$ be a stencil of size $r_j \geq 2$ for $j = 0, 1, \ldots, \ell$. Assume that $r_0 \leq r_1 \leq \cdots \leq r_\ell$. Let α^{r_j} be the positive linear weights such that $\sum_j \alpha^{r_j} = 1$, and let σ^{r_j} be the corresponding smoothness indicators. If u is smooth except for a single discontinuity, and if u is smooth on at least one stencil, then for grids bounded away from the discontinuity,*

$$\tilde{\alpha}^{r_j} = \begin{cases} \Theta(1) & \text{if } u \text{ is smooth on } S^{r_j}, \\ \Theta(h^{2\eta}) & \text{if } u \text{ has a jump discontinuity on } S^{r_j} \end{cases} \tag{5.4}$$

for all $j = 0, 1, \ldots, \ell$, for both WENO-JS and WENO-Z weights provided $\tau = \Theta(1)$.

We remark that the WENO-Z weights defined in (2.9) for standard WENO require $r \geq 3$. When r is odd, $\tau = \Theta(1)$, since $\tau = |\sigma_{-k} - \sigma_k|$, $k = \lfloor \frac{r}{2} \rfloor$, compares the leftmost and rightmost stencils, only one of which contains the discontinuity. It is not clear whether $\tau = \Theta(1)$ when r is even in (2.9).

Proof. First consider the WENO-JS weights. By (2.6), Lemmas 4.1 and 5.2, for any $j \neq k$,

$$\frac{\sigma^{r_j} - \sigma^{r_k}}{\sigma^{r_k} + \epsilon_h} = \begin{cases} \mathcal{O}(h^{\min(r_j, r_k) - 1}) & \text{if } u \text{ is smooth on } S^{r_j} \text{ and } S^{r_k}, \\ \Theta(1) & \text{if } u \text{ is smooth on } S^{r_j}, \text{ but jumps on } S^{r_k}, \\ \Theta(h^{-2}) & \text{if } u \text{ jumps on } S^{r_j}, \text{ but is smooth on } S^{r_k}, \\ \mathcal{O}(1) & \text{if } u \text{ jumps on } S^{r_j} \text{ and } S^{r_k}. \end{cases}$$

Hence we obtain

$$\sum_{k=0}^{\ell} \alpha^{r_k} \Big(1 + \frac{\sigma^{r_j} - \sigma^{r_k}}{\sigma^{r_k} + \epsilon_h} \Big)^{\eta} = \begin{cases} \Theta(1) & \text{if } u \text{ is smooth on } S^{r_j}, \\ \Theta(h^{-2\eta}) & \text{if } u \text{ jumps on } S^{r_j}, \end{cases} \tag{5.5}$$

and so (4.7) and (5.5) imply the result (5.4).

For the WENO-Z weights, since $\tau = \Theta(1)$, (4.8) shows

$$\rho_{r_j} = \frac{\tau}{\sigma^{r_j} + \epsilon_h} = \begin{cases} \Theta(h^{-2}) & \text{if } u \text{ is smooth on } S^{r_j}, \\ \Theta(1) & \text{if } u \text{ jumps on } S^{r_j}. \end{cases} \tag{5.6}$$

Thus the denominator in (4.11) is dominated by $\Theta(h^{-2})$, and the result follows. ∎

We present in the next theorems the accuracy of the WENO reconstructions. The first theorem is a generalization of a result in [1].

5.2.1. Standard WENO and WENO-AO(r, s).

THEOREM 5.5. *Let $K > 0$ and $\epsilon_h = Kh^2$. Given cell I_i, let u be smooth except for a jump discontinuity $x_* \in I_m$, $m \neq i$. Assume that the grids are bounded away from the discontinuity and that WENO-JS weights or WENO-Z weights are used, where in the latter case $\tau = \Theta(1)$. For the standard WENO reconstruction R_r, $r = 2s - 1$, $s \geq 2$, for the point x^* in (3.1), where $I_m \in S_0^{2s-1}$,*

$$|R_r(x^*) - u(x^*)| = \mathcal{O}(h^s) \quad \text{if} \quad \eta \geq s/2. \tag{5.7}$$

For the WENO-AO(r, s) reconstruction $R^{r,s}$, $r > s \geq 2$, where $I_m \in S_0^r$ and $I_i \in S_j^s \subseteq S_0^r$, for all j, on I_i,

$$|R^{r,s}(x) - u(x)| = \mathcal{O}(h^s) \quad \forall x \in I_i \quad \text{if} \quad \eta \geq s/2. \tag{5.8}$$

Proof. For either weights, we have

$$\begin{aligned}
|R_r(x^*) - u(x^*)| &= \Big|\sum_j \tilde{\alpha}_j^s (P_j^s(x^*) - u(x^*))\Big| \\
&\le \sum_{\substack{u \text{ discontin-}\\ \text{uous on } S_j^s}} \tilde{\alpha}_j^s \big|P_j^s(x^*) - u(x^*)\big| + \sum_{\substack{u \text{ smooth}\\ \text{on } S_j^s}} \tilde{\alpha}_j^s \big|P_j^s(x^*) - u(x^*)\big| \\
&= \Theta(h^{2\eta})\,\mathcal{O}(1) + \Theta(1)\,\mathcal{O}(h^s).
\end{aligned}$$

by Theorem 5.4, and (5.7) follows. Again using Theorem 5.4, we also compute

$$\begin{aligned}
&|R^{r,s}(x) - u(x)| \\
&\quad\le \left|\frac{\tilde{\alpha}_0^r}{\alpha_0^r}\Big[(P_0^r(x) - u(x)) - \sum_j \alpha_j^s (P_j^s(x) - u(x))\Big]\right| + \sum_j \tilde{\alpha}_j^s \big|P_j^s(x) - u(x)\big| \\
&\quad\le \mathcal{O}(\tilde{\alpha}_0^r)\,[\mathcal{O}(1) + \mathcal{O}(h^s)] + \left\{\sum_{\substack{u \text{ discontin-}\\ \text{uous on } S_j^s}} \mathcal{O}(\tilde{\alpha}_j^s)\,\mathcal{O}(1) + \sum_{\substack{u \text{ smooth}\\ \text{on } S_j^s}} \mathcal{O}(\tilde{\alpha}_j^s)\,\mathcal{O}(h^s)\right\} \\
&\quad= \Theta(h^{2\eta})\,[\mathcal{O}(1) + \mathcal{O}(h^s)] + \left\{\sum_{\substack{u \text{ discontin-}\\ \text{uous on } S_j^s}} \Theta(h^{2\eta})\,\mathcal{O}(1) + \sum_{\substack{u \text{ smooth}\\ \text{on } S_j^s}} \Theta(1)\,\mathcal{O}(h^s)\right\}.
\end{aligned}$$

Therefore we conclude the result (5.8). ∎

The example below shows that when there is a jump discontinuity bounded away from the gridpoint on the big stencil, the standard WENO reconstruction R_r and the WENO-AO(r,s) reconstruction may not drop to order s when $\eta < s/2$. That is, the requirement that $\eta \ge s/2$ is sharp.

Example 5.6. Given cell $I_i = \big[\frac{h}{2}, \frac{3h}{2}\big]$ and u defined by (5.3), consider the stencil $S_0^5 = \big\{[\frac{-3h}{2}, \frac{-h}{2}], [\frac{-h}{2}, \frac{h}{2}], I_i, [\frac{3h}{2}, \frac{5h}{2}], [\frac{5h}{2}, \frac{7h}{2}]\big\}$. The average of u on each cell is 1, 1/2, 0, 0, and 0, respectively. Consider the standard WENO reconstruction R_3 and the WENO-AO$(5,3)$ reconstruction with $\epsilon_h = h^2$. The stencil polynomials are

$$P_{-1}^3(x) = \frac{1}{2} - \frac{x}{2h}, \quad P_0^3 = \frac{23}{48} - \frac{3x}{4h} + \frac{x^2}{4h^2}, \quad P_1^3 = 0,$$
$$P_0^5(x) = \frac{317}{640} - \frac{17x}{24h} + \frac{x^2}{16h^2} + \frac{x^3}{6h^3} - \frac{x^4}{24h^4}.$$

Therefore, the errors at $x = h/2$ (the leftmost point of I_i) are

$$P_{-1}^3\Big(\frac{h}{2}\Big) - u\Big(\frac{h}{2}\Big) = \frac{1}{4} = \Theta(1), \quad P_0^3\Big(\frac{h}{2}\Big) - u\Big(\frac{h}{2}\Big) = \frac{1}{6} = \Theta(1),$$
$$P_1^3\Big(\frac{h}{2}\Big) - u\Big(\frac{h}{2}\Big) = 0, \quad P_0^5\Big(\frac{h}{2}\Big) - u\Big(\frac{h}{2}\Big) = \frac{7}{40} = \Theta(1),$$

and the smoothness indicators are

$$\sigma_{-1}^3 = \frac{1}{4} = \Theta(1), \quad \sigma_0^3 = \frac{1}{3} = \Theta(1), \quad \sigma_1^3 = 0, \quad \sigma_0^5 = \frac{30593}{20160} = \Theta(1).$$

By Theorem 5.4, since $\tau = \Theta(1)$, for both weights, we have

TABLE 5.1
Example 5.6, Standard WENO R_3 and WENO-AO(5,3) error and convergence rate at $x = h/2$. The convergence rates are indeed $\Theta(h^{2\eta})$.

	$\eta = 1$		$\eta = 1.5$		$\eta = 2$		$\eta = 3$	
n	Error	Order	Error	Order	Error	Order	Error	Order
Standard WENO R_3, WENO-JS								
6	1.45E-3	1.97	4.26E-5	2.99	1.25E-6	3.99	1.09E-9	5.99
7	3.65E-4	1.99	5.34E-6	3.00	7.82E-8	4.00	1.70E-11	6.00
8	9.15E-5	2.00	6.67E-7	3.00	4.89E-9	4.00	2.66E-13	6.00
9	2.29E-5	2.00	8.34E-8	3.00	3.06E-10	4.00	4.16E-15	6.00
Standard WENO R_3, WENO-Z								
6	3.12E-3	1.93	9.60E-5	2.99	2.92E-6	4.00	2.72E-9	6.00
7	7.90E-4	1.98	1.20E-5	3.00	1.83E-7	4.00	4.25E-11	6.00
8	1.98E-4	2.00	1.50E-6	3.00	1.14E-8	4.00	6.64E-13	6.00
9	4.96E-5	2.00	1.88E-7	3.00	7.13E-10	4.00	1.04E-14	6.00
WENO-AO(5,3), WENO-JS								
6	8.58E-4	1.98	1.72E-5	3.00	4.07E-7	3.99	3.10E-10	5.99
7	2.15E-4	1.99	2.15E-6	3.00	2.55E-8	4.00	4.86E-12	6.00
8	5.39E-5	2.00	2.69E-7	3.00	1.59E-9	4.00	7.60E-14	6.00
9	1.35E-5	2.00	3.36E-8	3.00	9.95E-11	4.00	1.19E-15	6.00
WENO-AO(5,3), WENO-Z								
6	1.50E-3	1.96	2.60E-5	3.00	5.26E-7	3.99	3.32E-10	5.99
7	3.76E-4	1.99	3.25E-6	3.00	3.29E-8	4.00	5.20E-12	6.00
8	9.42E-5	2.00	4.06E-7	3.00	2.06E-9	4.00	8.13E-14	6.00
9	2.36E-5	2.00	5.08E-8	3.00	1.29E-10	4.00	1.27E-15	6.00

$$\tilde{\alpha}^3_{-1} = \Theta(h^{2\eta}), \quad \tilde{\alpha}^3_0 = \Theta(h^{2\eta}), \quad \tilde{\alpha}^5_0 = \Theta(h^{2\eta}).$$

So the error of the reconstruction R_3 at $x = h/2$ is

$$R_3\Big(\frac{h}{2}\Big) - u\Big(\frac{h}{2}\Big) = \sum_{j=-1}^{1} \tilde{\alpha}^3_j \Big[P^3_j\Big(\frac{h}{2}\Big) - u\Big(\frac{h}{2}\Big)\Big] = \mathcal{O}(h^{2\eta}) \le \Theta(h^{2\eta}).$$

On the other hand, for $R^{5,3}$ at $x = h/2$,

$$R^{5,3}\Big(\frac{h}{2}\Big) - u\Big(\frac{h}{2}\Big) = \frac{\tilde{\alpha}^5_0}{\alpha^5_0}\Big\{\Big[P^5_0\Big(\frac{h}{2}\Big) - u\Big(\frac{h}{2}\Big)\Big] - \sum_{j=-1}^{1} \alpha^3_j \Big[P^3_j\Big(\frac{h}{2}\Big) - u\Big(\frac{h}{2}\Big)\Big]\Big\}$$
$$+ \sum_{j=-1}^{1} \tilde{\alpha}^3_j \Big[P^3_j\Big(\frac{h}{2}\Big) - u\Big(\frac{h}{2}\Big)\Big] = \mathcal{O}(h^{2\eta}) \le \Theta(h^{2\eta}).$$

Numerical results in Table 5.1 show that we can achieve $\Theta(h^{2\eta})$ convergence for R_3 and WENO-AO(5,3) for $\eta = 1, 1.5, 2, 3$. When $\eta = 1$, both of the reconstructions are only second order accurate instead of third for either WENO-JS or WENO-Z weights. We used the sequence of grid spacings $\{h_n = 2^{-n}\}_{n=0}^{\infty}$ and $\alpha^5_0 = 0.85$, $\alpha^3_j = 0.05$ for these results.

5.2.2. Multilevel WENO-AO$_s(r_\ell, \dots, r_1, s)$. We have the following result for the multilevel WENO-AO$_s(r_\ell, \dots, r_0, s)$ reconstructions.

THEOREM 5.7. *Let $K > 0$ and $\epsilon_h = Kh^2$. Let cell I_i be given, $\ell \ge 2$, $r_\ell > r_{\ell-1} > \cdots > r_0 = s \ge 2$, and $I_i \in S^{r_0}_j \subseteq S^{r_1}_0 \subseteq \cdots \subseteq S^{r_\ell}_0$ for all j. Let u be smooth except for a jump discontinuity at $x_* \in I_m \in S^{r_\ell}_0$, $m \ne i$. Assume that $x_* \in S^{r_{n+1}}_0$ but $x_* \notin S^{r_n}_j$,*

$0 \le n < \ell$ ($j = 0$ if $r_n \ge 1$) and that WENO-JS weights or WENO-Z weights are used with variable η_k. Then for the WENO-AO$_s(r_\ell, \dots, r_1, s)$ reconstruction, the following hold on grids bounded away from the discontinuity:

1. *If $n = \ell - 1$, let $q = \min(r_{\ell-1}, r_{\max}(\eta_{\ell-1}))$, where $r_{\max}$ is given in Theorem 4.4. If $\eta_\ell \ge (q-s)/2$, $\eta_{0,\ell} \ge s/2$, and (4.20)–(4.22) hold with ℓ replaced by $\ell - 1$, then on I_i,*

$$|R_s^{r_\ell,\dots,r_1,s}(x) - u(x)| = \mathcal{O}(h^q) \quad \forall x \in I_i. \tag{5.9}$$

2. *If $n < \ell - 1$ and $\eta_{0,k} \ge s/2$, $1 \le k \le \ell$, then on I_i,*

$$|R_s^{r_\ell,\dots,r_1,s}(x) - u(x)| = \mathcal{O}(h^s) \quad \forall x \in I_i. \tag{5.10}$$

Note that WENO-AO$_s(r_\ell, \dots, r_1, s)$ drops to the base order s when u has a jump discontinuity on the two biggest stencils.

Proof. If $n = \ell - 1$, then $\tau = |\sigma^{r_\ell} - \sigma^{r_{\ell-1}}| = \Theta(1)$ by (2.6) and Lemma 5.2. By Theorem 5.4, $\tilde\gamma^{r_\ell,s} = \Theta(h^{2\eta_\ell})$ and $\tilde\gamma^{r_{\ell-1},\dots,r_1,s} = \Theta(1)$. Following (4.23) and using Theorems 4.5 and 5.5,

$$\begin{aligned}
&|R_s^{r_\ell,\dots,r_1,s}(x) - u(x)| \\
&\quad \le \left| \frac{\tilde\gamma^{r_\ell,s}}{\gamma^{r_\ell,s}} \left[(R_s^{r_\ell,s}(x) - u(x)) - \gamma^{r_{\ell-1},\dots,r_1,s}(R_s^{r_{\ell-1},\dots,r_1,s}(x) - u(x)) \right] \right| \\
&\qquad + \left| \tilde\gamma^{r_{\ell-1},\dots,r_1,s}(R_s^{r_{\ell-1},\dots,r_1,s}(x) - u(x)) \right| \\
&\quad \le \Theta(\tilde\gamma^{r_\ell,s}) \left[\mathcal{O}(h^s) + \mathcal{O}(h^q) \right] + \Theta(\tilde\gamma^{r_{\ell-1},\dots,r_1,s})\, \mathcal{O}(h^q) \\
&\quad = \Theta(h^{2\eta_\ell})\, \mathcal{O}(h^s) + \Theta(1)\, \mathcal{O}(h^q).
\end{aligned} \tag{5.11}$$

Since $q \ge s$, we conclude (5.9).

When $0 \le n < \ell - 1$, u is smooth neither on $S_0^{r_\ell}$ nor on $S_0^{r_{\ell-1}}$, so Lemma 5.2 shows $\sigma^{r_\ell} = \Theta(1)$ and $\sigma^{r_{\ell-1}} = \Theta(1)$. Hence, following (3.8), (3.11), and (3.9), $\tilde\gamma^{r_\ell,s} = \Theta(1)$ and $\tilde\gamma^{r_{\ell-1},\dots,r_1,s} = \Theta(1)$. Since $R_s^{r_\ell,s}(x)$ and $R_s^{r_{\ell-1},\dots,r_1,s}(x)$ is at least order s accurate when $\eta_{0,k} \ge s/2$, $1 \le k \le \ell$, then an argument similar to (5.11) shows (5.10). ∎

5.2.3. The new multilevel WENO-AO$(r_\ell, \dots, r_0)$. When u is smooth only on some substencils of $S_0^{r_\ell}$, we have the following result for the new reconstruction.

THEOREM 5.8. *Let $K > 0$ and $\epsilon_h = Kh^2$. Let cell I_i be given, $\ell \ge 2$, $r_\ell > r_{\ell-1} > \cdots > r_0 \ge 2$, and $I_i \in S_j^{r_0} \subseteq S_0^{r_1} \subseteq \cdots \subseteq S_0^{r_\ell}$ for all j. Let u be smooth except for a jump discontinuity at $x_* \in I_m \in S_0^{r_\ell}$, $m \ne i$. Assume that $x_* \in S_0^{r_{n+1}}$ but $x_* \notin S_j^{r_n}$, $0 \le n < \ell$ ($j = 0$ if $r_n \ge 1$) and that WENO-JS weights or WENO-Z weights are used with variable η_k. Then on grids bounded away from the discontinuity, the WENO-AO$(r_\ell, \dots, r_0)$ reconstruction satisfies on I_i,*

$$|R^{r_\ell,\dots,r_0}(x) - u(x)| = \mathcal{O}(h^p) \quad \text{if } \eta_k \ge p/2,\ n+1 \le k \le \ell, \tag{5.12}$$

where $p = \min(r_n, r_{\max,n})$ with $r_{\max,n}$ being given in (4.25). Moreover, if $r_k \le r_{\max,k}$ for each $1 \le k \le n$ and $q > 0$ is fixed, then on I_i,

$$|R^{r_\ell,\dots,r_0}(x) - u(x)| = \mathcal{O}(h^{\min(q,r_n)}) \quad \text{if } \eta_k \ge q/2,\ n+1 \le k \le \ell. \tag{5.13}$$

Thus, if $q = r_{\ell-1}$, the reconstruction drops to the best order possible. A smaller value of q may be chosen to keep the collection of η_k from becoming too large.

Proof. Following (4.27),

$$
\begin{aligned}
&|R^{r_\ell,\dots,r_0}(x)-u(x)| \\
&\quad\le \frac{\tilde\alpha_0^{r_\ell}}{\alpha_0^{r_\ell}}\Big[|P_0^{r_\ell}(x)-u(x)|+\Big(\sum_j \alpha_j^{r_0}\Big)|R^{r_{\ell-1},\dots,r_0}(x)-u(x)|\Big] \\
&\qquad+\Big(\sum_j \tilde\alpha_j^{r_0}\Big)|R^{r_{\ell-1},\dots,r_0}(x)-u(x)|.
\end{aligned}
\tag{5.14}
$$

We will prove the result by induction on $\ell \ge n+1$. When $\ell = n+1$, by Theorems 4.6 and 5.4, we have

$$
\begin{aligned}
&|R^{r_\ell,\dots,r_0}(x)-u(x)| \\
&\quad\le \Theta(\tilde\alpha_0^{r_\ell})\big[\mathcal{O}(1)+\mathcal{O}(h^{\min(r_{\ell-1},r_{\max,\ell-1})})\big]+\Big(\sum_j \Theta(\tilde\alpha_j^{r_0})\Big)\mathcal{O}(h^{\min(r_{\ell-1},r_{\max,\ell-1})}) \\
&\quad=\Theta(h^{2\eta_\ell})\,\mathcal{O}(1)+\Theta(1)\,\mathcal{O}(h^p).
\end{aligned}
\tag{5.15}
$$

So the result holds when $\ell = n+1$. Assume by induction that the result holds for some $\ell-1 \ge n+1$. Then $|R^{r_{\ell-1},\cdots,r_0}(x)-u(x)| = \mathcal{O}(h^p)$, so by an argument similar to (5.15), we conclude the result (5.12) holds for ℓ. Result (5.13) is shown in a similar way. ∎

5.3. Discussion. WENO philosophy desires that our reconstructions be high order accurate when the solution is smooth and yet maintain low order accuracy when there is a discontinuity *not* in the central cell I_i. For the latter, it is required that $\epsilon_h = Kh^2$ [1]. We summarize and discuss the results when either the solution is smooth or there is a discontinuity *not* in the central cell I_i, but the grids are then bounded away from the discontinuity.

Theorems 5.5 and 4.3 together show that, given any s, the standard WENO reconstruction R_r, $r = 2s-1$, behaves as desired. It is high order accurate, i.e., order $r = 2s-1$, when the solution is smooth, and it drops to low order, i.e., order s, when there is a discontinuity not on I_i, provided only that we satisfy a condition on η. This condition, given originally in [1], is that $\eta \ge s/2$. We showed that this condition is sharp.

Theorems 5.5 and 4.4 together show that the two-level WENO-AO(r,s) reconstructions can achieve higher order r accuracy in the smooth case and otherwise maintain at least order s accuracy. For WENO-JS weights, we simply require that $r \le 2s-1$ and $\eta \ge s/2$. WENO-Z weights are more complex, and we require that τ be chosen so as to have $\tau = \Theta(1)$ in the discontinuous case. Now, we require that $r \le 2s-1+(s-1)\eta$ and $\eta \ge s/2$, so any r and s can be used, at the expense of requiring η to be very large.

For the multilevel WENO-AO$_s(r_\ell,\dots,r_1,s)$, we have Theorems 4.5 and 5.7. The latter theorem tells us that in the discontinuous case, when the discontinuity lies within the two biggest stencils, the multilevel reconstruction reduces to the base order s, independently of how the multiple levels are treated. For WENO-JS weights, we require $r_\ell \le 2s-1$ and all the base reconstructions WENO-AO$_s(r_k,s)$ to be accurate, so we are required to take $\eta_{0,k} \ge s/2$. The multilevel reconstruction is no better than the two-level one when WENO-JS weights are used. When WENO-Z weights are used, the accuracy in the smooth case can be as high as we like, provided enough intermediate levels or large enough η are taken to satisfy (4.21)–(4.22), and provided $\eta_{0,k}$ are taken so very large that (4.20) holds.

The new multilevel WENO-AO$(r_\ell,\dots,r_1,s)$ behaves better. In the smooth case, we have order r_ℓ accuracy provided that the levels satisfy (4.26). Moreover, in the nonsmooth case, the reconstruction drops to a lower order depending on exactly where the discontinuity lies. So if the discontinuity is in stencil $S_0^{r_{n+1}}$ but not in $S_0^{r_n}$ (or some $S_j^{r_0}$ when $n=0$), then we drop to order r_n, provided that $\eta_k \ge r_\ell/2$ for each k. Since this latter condition forces large values of η (which may be undesirable as noted at the end of section 4.3.5), one can make the reconstruction drop to order $\min(s,r_n)$ for any s provided only that $\eta_k \ge s/2$ for each k.

6. A cautionary example of a discontinuity not bounded away from the gridpoints. Now we consider grids for which the discontinuity x_* is not bounded away from the gridpoints. The following example shows that, in exact arithmetic, the WENO reconstruction may not drop to the accuracy of the smallest stencil, as the philosophy of WENO expects.

Let $u(x)=H(x_*-x)$ be a simple step function with a discontinuity at x_*, where

$$x_* = \sum_{k=0}^{\infty} 2^{-2^k} = 0.110\overset{k=2}{1}\underbrace{000}_{3}\overset{k=3}{1}\underbrace{0000000}_{7}\overset{k=4}{1}\underbrace{000000000000000}_{15}\overset{k=5}{1}000\cdots \tag{6.1}$$

in binary. We use the sequence of grid spacings $\{h_n\}_{n=1}^\infty$, where $h=h_n=2^{-n}$, and grids $\{x_k^h=kh\}_{k=-\infty}^{\infty}$. Let $x_*\in[x_m^h,x_{m+1}^h)$ and define $c(h)$ so $x_*=x_m^h+c(h)h$, i.e.,

$$c(h)=\frac{x_*-x_m^h}{h}=2^n x_* - m = \sum_{k=0}^{\infty} 2^{n-2^k} - m.$$

The gridpoints have only n digits after the binary point, so $\liminf_{h\to 0} c(h)=0$ and the gridpoints are *not* bounded away from the discontinuity. Our sequence of grids gives rise to three subsequences as follows:

(1) For the subsequence $\{h_n : n=2^\ell,\ \ell=0,\dots,\infty\}$, we have $c(h_n)=\Theta(h_n)$ as $\ell\to\infty$. That is, x_* gets closer to the gridpoints when the grid is refined.
(2) For the subsequence $\{h_n : 2^\ell < n < 2^{\ell+1}, \ell=2,\dots,\infty\}$, we have $2^{-2^{\ell+1}} \le c(h_n)h_n \le 2^{-2^\ell}$. For each n between its limits 2^ℓ and $2^{\ell+1}$, we abuse notation by writing $c(h_n)=\Theta(h_n^{-1})$, but this holds only for finite, contiguous segments of the subsequence.
(3) For the subsequence $\{h_n : n=2^\ell-1,\ \ell=2,\dots,\infty\}$, we have $c(h_n)=\Theta(1)$ as $n\to\infty$. This subsequence of grids has x_* bounded away from the gridpoints.

We consider the WENO-AO(3,2) reconstruction with WENO-JS weights and $\epsilon_h = h^2$. Let

$$S_0^3=\{[x_m^h,x_{m+1}^h],[x_{m+1}^h,x_{m+2}^h],[x_{m+2}^h,x_{m+3}^h]\},$$

that is, the jump discontinuity lies in the leftmost cell of S_0^3. The average on each cell is $c(h)$, 0, and 0, respectively. Then the stencil polynomials are

$$P_0^2(x) = -\frac{c(h)}{h}\left(x-x_m^h-\frac{3h}{2}\right),\quad P_1^2(x)=0,$$

$$P_0^3(x) = -\frac{c(h)}{24}-\frac{c(h)}{2h}\left(x-x_m^h-\frac{3h}{2}\right)+\frac{c(h)}{2h^2}\left(x-x_m^h-\frac{3h}{2}\right)^2.$$

Therefore, the errors at, say, $x = x_m^h + h = x_{m+1}^h$ are

$$P_0^2(x_{m+1}^h) - u(x_{m+1}^h) = \Theta(c(h)), \quad P_1^2(x_{m+1}^h) - u(x_{m+1}^h) = 0, \\ P_0^3(x_{m+1}^h) - u(x_{m+1}^h) = \Theta(c(h)), \tag{6.2}$$

and the smoothness indicators are

$$\sigma_0^2 = c(h)^2 = \Theta(c(h))^2, \quad \sigma_1^2 = 0, \quad \sigma_0^3 = \frac{4}{3}c(h)^2 = \Theta(c(h))^2. \tag{6.3}$$

Using (2.7) and (2.8), we compute that

$$\tilde{\alpha}_0^2 \quad \text{and} \quad \tilde{\alpha}_0^3 = \begin{cases} \Theta(1) & \text{if } c(h) = \Theta(h), \\ \Theta(h^{4\eta}) & \text{if } c(h) = \Theta(h^{-1}), \\ \Theta(h^{2\eta}) & \text{if } c(h) = \Theta(1). \end{cases}$$

So the error of the reconstruction $R^{3,2}$ at x_{m+1}^h is

$$\begin{aligned} &R^{3,2}(x_{m+1}^h) - u(x_{m+1}^h) \\ &\quad = \frac{\tilde{\alpha}_0^3}{\alpha_0^3}\Big[\big(P_0^3(x_{m+1}^h) - u(x_{m+1}^h)\big) - \sum_{j=0}^{1} \alpha_j^2\big(P_j^2(x_{m+1}^h) - u(x_{m+1}^h)\big)\Big] \\ &\qquad + \sum_{j=0}^{1} \tilde{\alpha}_j^2\big(P_j^2(x_{m+1}^h) - u(x_{m+1}^h)\big) \\ &\quad = \begin{cases} \mathcal{O}(h) & \text{if } c(h) = \Theta(h), \\ \mathcal{O}(h^{4\eta-1}) & \text{if } c(h) = \Theta(h^{-1}), \\ \mathcal{O}(h^{2\eta}) & \text{if } c(h) = \Theta(1). \end{cases} \end{aligned} \tag{6.4}$$

We illustrate the results (6.2)–(6.4) numerically, using high-precision arithmetic. In Figures 6.1–6.3, the black dots are the logarithm of the smoothness indicators and errors to base 2, respectively. The red, green, and blue dashed lines connect the grids in subsequences (1), (2), and (3), where $c(h) = \Theta(h)$, $\Theta(h^{-1})$, and $\Theta(1)$, respectively. The negative value of the slope is the convergence rate, computed over the subsequence for subsequences (1) and (3) and the contiguous segments of the subsequences (2).

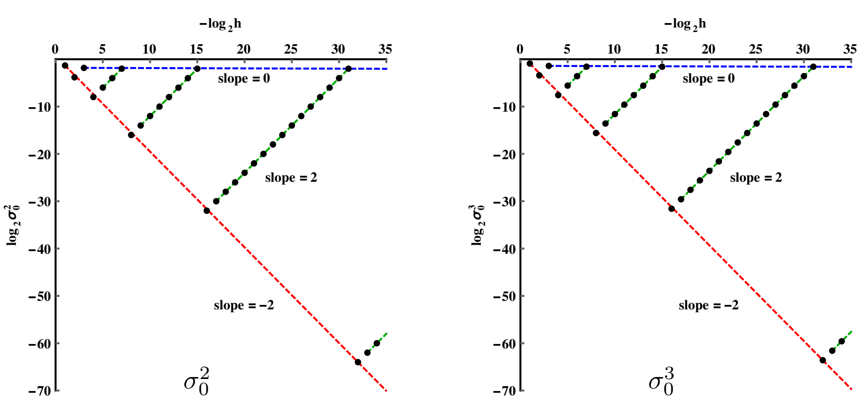

FIG. 6.1. *Log-log plot of smoothness indicators.*

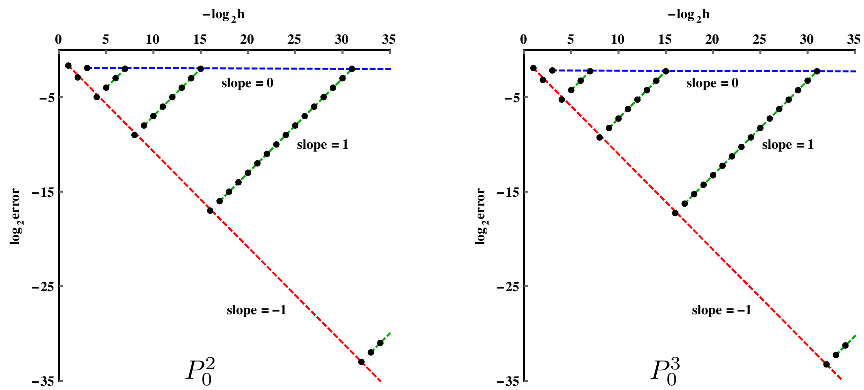

FIG. 6.2. *Log-log plot of the polynomial approximation error.*

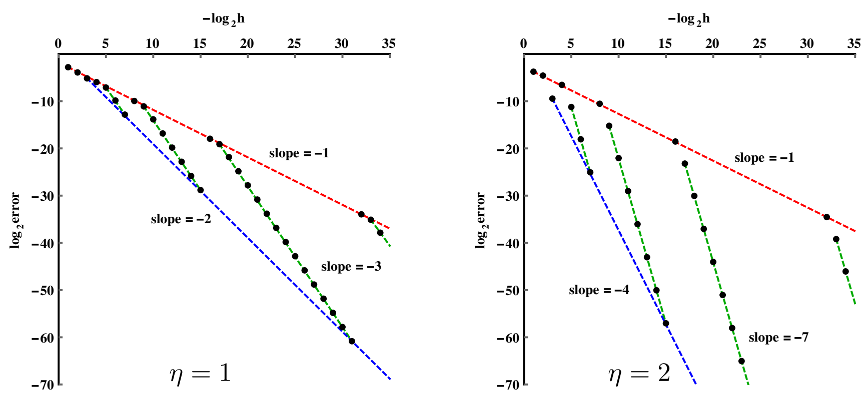

FIG. 6.3. *Log-log plot of the $R^{3,2}$ reconstruction error.*

Figure 6.1 shows that the smoothness indicators of σ_0^2 and σ_0^3 indeed have order 2 in subsequence (1), order -2 in subsequence (2), and order 0 in subsequence (3). Figure 6.2 shows the stencil polynomials P_0^2 and P_0^3 approximate to order 1, -1, and 0 in subsequences (1), (2), and (3), respectively. Figure 6.3 shows the reconstruction $R^{3,2}$ approximates to only first order in subsequence (1), and this is the best we can guarantee in general. The rate improves in subsequence (2) to order 3 when $\eta = 1$ and order 7 when $\eta = 2$. As expected for subsequence (3), when the grids are bounded away from the discontinuity, we see order 2 when $\eta = 1$, and we see the improved order 4 when $\eta = 2$.

We have shown there exist sequences of grids for which the results in section 5.2 are violated. We are concerned with how often this situation arises. Without loss of generality, consider the same grid spacings $h = h_n = 2^{-n}$, $n = 0, 1, \ldots, \infty$. We assume that x_* lies at an arbitrary position within its grid cell, so it is uniformly distributed within this cell in the sense of probability. We need only compute the probability that x_* is like the point in (6.1), i.e., $c(h)$ is not uniformly bounded below by some positive number. If x_* is written in binary, then we need the number to have an increasing maximum number of consecutive zero digits. We compute the probability

$$\begin{aligned}
&\text{Prob}(x_* \text{ has increasing maximum number of consecutive 0's})\\
&\quad = 1 - \text{Prob}(x_* \text{ has fixed maximum number of consecutive 0's})\\
&\quad = 1 - \sum_{\ell=0}^{\infty} \text{Prob}(x_* \text{ has maximum number } \ell \text{ of consecutive 0's}) = 1.
\end{aligned}$$

This shows that almost surely the gridpoints are not bounded away from the discontinuity, if exact arithmetic is used, as we refine the grid.

This result is not particularly disconcerting for WENO schemes for solving (1.1), however. Trivially, we use finite precision arithmetic, which sets an artificial lower bound on how close x_* can be to the gridpoints. More importantly, however, we solve a given problem on only one or perhaps a few grids, but consider the solution in time. Suppose we arbitrarily set $c_* = 0.001$. As the shock or contact discontinuity moves in time, assuming a uniform probability for its position with respect to the grid, there is a 99.8% chance that the discontinuity x_* is bounded away from the gridpoints (independently of h). That is, within a WENO scheme, the situation described in this cautionary example does not arise often. It is already clear that there is a single big stencil with center cell I_i containing x_* for which u is not smooth on any small stencil, so WENO reconstruction does not give a good result on that cell. The example shows that there may be a few other cells arising from time to time that have poor approximation.

WENO reconstruction still captures the discontinuity, as is well known from numerical tests. In fact, we saw above that as $h \to 0$, if $\sigma \to 0$ on some stencil S^r, then P^r converges smoothly to a constant. WENO reconstruction will include this stencil, but picking it up will give a good reconstruction, albeit not to the order we had desired.

7. Numerical results in one space dimension. In our one-dimensional tests of the conservation law (1.1), the L^1 and L^∞ errors are computed, respectively, by

$$\sum_i \left| \frac{1}{\Delta x_i} \int_{I_i} u(x,t^n)\ dx - \bar{u}_i^n \right| \Delta x_i \quad \text{and} \quad \max_i \left| \frac{1}{\Delta x_i} \int_{I_i} u(x,t^n)\ dx - \bar{u}_i^n \right|.$$

7.1. Reconstruction near jump discontinuities. Our first test case is from [9, 1, 11]. Recall that H is the Heaviside function. For x_* fixed, let

$$u(x) = g(x) + H(x_* - x).$$

Consider the grid spacings $\{h_n\}_{n=0}^{\infty}$, where $h_n = 0.1/2^n$, and fix $I_i = [0, h_n]$. We test the accuracy of WENO-AO$_3(9,7,5,3)$ and WENO-AO$(9,7,5,3)$ reconstructions at $x = 0$ when $x_* = -4h, -3h, -2h$, and $-h$. That is, u is smooth only on S_0^9, S_0^7, S_0^5, and S_j^3, respectively, where $j = 0, 1$.

We first take $g(x) = x^3 + \sin(x)$, so $g'(0) \neq 0$. The results are shown in Table 7.1 for WENO-JS weights and Table 7.2 for WENO-Z weights. We set our algorithm parameters based on Theorems 5.5 and 5.7 (see also the discussion in section 5.3). We take $\epsilon_h = h^2$ for both of WENO-JS and WENO-Z weights.

For WENO-AO$_3(9,7,5,3)$, we use in the two-level base reconstructions the linear weights 0.85 for the big stencil and 0.05 for the three small stencils, and $\eta_{0,k} = 2 > s/2 = 3/2$. For the recursive levels, the higher order linear weight is 0.85 and 0.15 is the other weight. For the recursive level $r_2 = 7$, $\eta_2 = 1 = (r_1 - s)/2$, where $r_1 = 5$. For level $r_3 = 9$, $\eta_3 = 2 = (r_2 - s)/2$.

TABLE 7.1
Example 7.1 *with* $g(x) = x^3 + sin(x)$. *WENO-JS weights with* $\epsilon_h = h^2$. *Error and convergence rate at* $x = 0$.

n	$x_* = -4h$ Error	Order	$x_* = -3h$ Error	Order	$x_* = -2h$ Error	Order	$x_* = -h$ Error	Order
				$\text{WENO}_3(9,7,5,3)$				
6	2.91E-15	5.00	2.91E-15	5.00	4.25E-12	3.04	1.58E-9	3.00
7	9.09E-17	5.00	9.10E-17	5.00	5.27E-13	3.01	1.98E-10	3.00
8	2.84E-18	5.00	2.84E-18	5.00	6.58E-14	3.00	2.48E-11	3.00
9	8.88E-20	5.00	8.88E-20	5.00	8.22E-15	3.00	3.10E-12	3.00
				$\text{WENO}(9,7,5,3)$				
6	3.57E-27	9.00	2.89E-21	7.00	3.07E-15	5.00	1.58E-9	2.99
7	6.97E-30	9.00	2.26E-23	7.00	9.58E-17	5.00	1.98E-10	3.00
8	1.36E-32	9.00	1.76E-25	7.00	2.99E-18	5.00	2.48E-11	3.00
9	2.66E-35	9.00	1.38E-27	7.00	9.36E-20	5.00	3.10E-12	3.00

TABLE 7.2
Example 7.1 *with* $g(x) = x^3 + sin(x)$. *WENO-Z weights with* $\epsilon_h = h^2$. *Error and convergence rate at* $x = 0$.

n	$x_* = -4h$ Error	Order	$x_* = -3h$ Error	Order	$x_* = -2h$ Error	Order	$x_* = -h$ Error	Order
				$\text{WENO}_3(9,7,5,3)$				
6	3.35E-26	9.00	2.38E-19	7.00	8.64E-12	3.04	1.58E-9	2.99
7	6.54E-29	9.00	1.86E-21	7.00	1.07E-12	3.01	1.98E-10	2.99
8	1.28E-31	9.00	1.45E-23	7.00	1.34E-13	3.00	2.48E-11	3.00
9	2.50E-34	9.00	1.14E-25	7.00	1.67E-14	3.00	3.10E-12	3.00
				$\text{WENO}(9,7,5,3)$				
6	4.41E-29	9.00	7.79E-23	6.94	1.61E-16	5.05	1.57E-9	2.98
7	8.60E-32	9.00	6.21E-25	6.97	4.93E-18	5.02	1.97E-10	2.99
8	1.68E-34	9.00	4.91E-27	6.98	1.53E-19	5.01	2.48E-11	3.00
9	3.28E-37	9.00	3.85E-29	6.99	4.76E-21	5.01	3.10E-12	3.00

WENO-AO$_3(9,7,5,3)$ drops to the accuracy of the base level 3 when u is not smooth on S_0^7, i.e., for the latter two values of x_*. Since $r_{\max} = 2s - 1 = 5$ in Theorem 4.4, we conclude that WENO-AO$_3(9,7,5,3)$ is only $\mathcal{O}(h^5)$ for WENO-JS weights when u is smooth on S_0^7 or the biggest stencil S_0^9. For WENO-Z weights, hypotheses (4.20)–(4.22) are satisfied, so the reconstruction achieves optimal order if u is smooth on S_0^7 or S_0^9. We see exactly these results in Tables 7.1–7.2.

For the new WENO-AO$(9,7,5,3)$, we take $\alpha_j^3 = 0.05$, $\alpha_0^{r_k} = 0.85$, and $\eta_k = \lceil \frac{r_k}{2} \rceil$, $k = 1,2,3$. Since (4.26) holds, the new reconstruction has the optimal order r_k, $k \geq 1$, for each recursive level if u is smooth on $S_0^{r_k}$, for both WENO-JS and WENO-Z weights. Again, we see these results in Tables 7.1–7.2.

For direct comparison to [9, 1, 11], we also show the results for $g(x) = x^3 + \cos(x)$ in Tables 7.3–7.4. Note that $g'(0) = 0$, so we are at a critical point and (2.5) shows that we may have somewhat better results, depending on how the WENO weighting is done. Indeed, we see some improvement in the order of accuracy. This example is actually quite special, and the improvement observed is due to superconvergence of the stencil polynomial approximations. The improvement is *not* due to a change in the order of the smoothness indicators, because $\epsilon_h = h^2$, and so the nomalizing factor $\epsilon_h + \sigma = \Theta(h^2)$ whether $\sigma = \mathcal{O}(h^2)$ or $\mathcal{O}(h^4)$. We can explain our observations by our theoretical results.

Apart from the discontinuity, the true solution $g(x)$ is a cubic plus the even function $\cos(x)$. The base level polynomials P_j^3 are degree 2 and so can approximate g to at best third order, because the x^3 term limits the approximation. However, the

TABLE 7.3
Example 7.1 with $g(x) = x^3 + cos(x)$. WENO-JS weights with $\epsilon_h = h^2$. Error and convergence rate at $x = 0$.

	$x_* = -4h$		$x_* = -3h$		$x_* = -2h$		$x_* = -h$	
n	Error	Order	Error	Order	Error	Order	Error	Order
				$\text{WENO}_3(9,7,5,3)$				
6	1.23E-17	5.99	1.23E-17	5.99	5.08E-12	3.02	1.91E-9	3.00
7	1.92E-19	5.99	1.93E-19	6.00	6.32E-13	3.00	2.38E-10	3.00
8	3.01E-21	6.00	3.02E-21	6.00	7.90E-14	3.00	2.98E-11	3.00
9	4.71E-23	6.00	4.71E-23	6.00	9.87E-15	3.00	3.73E-12	3.00
				$\text{WENO}(9,7,5,3)$				
6	3.11E-32	9.99	1.81E-25	8.15	1.25E-17	5.99	1.91E-9	3.00
7	3.05E-35	10.00	6.68E-28	8.08	1.96E-19	5.99	2.38E-10	3.00
8	2.98E-38	10.00	2.53E-30	8.04	3.07E-21	6.00	2.98E-11	3.00
9	2.91E-41	10.00	9.74E-33	8.02	4.80E-23	6.00	3.73E-12	3.00

TABLE 7.4
Example 7.1 with $g(x) = x^3 + cos(x)$. WENO-Z weights with $\epsilon_h = h^2$. Error and convergence rate at $x = 0$.

	$x_* = -4h$		$x_* = -3h$		$x_* = -2h$		$x_* = -h$	
n	Error	Order	Error	Order	Error	Order	Error	Order
				$\text{WENO}_3(9,7,5,3)$				
6	1.69E-32	10.60	7.14E-20	7.00	1.03E-11	3.02	1.90E-9	3.00
7	2.70E-35	9.29	5.58E-22	7.00	1.29E-12	3.00	2.38E-10	3.00
8	2.90E-38	9.87	4.36E-24	7.00	1.61E-13	3.00	2.98E-11	3.00
9	2.89E-41	9.97	3.41E-26	7.00	2.01E-14	3.00	3.72E-12	3.00
				$\text{WENO}(9,7,5,3)$				
6	3.13E-32	10.00	2.65E-25	8.00	5.64E-19	6.00	1.90E-9	3.00
7	3.06E-35	10.00	1.04E-27	8.00	8.81E-21	6.00	2.38E-10	3.00
8	2.98E-38	10.00	4.05E-30	8.00	1.38E-22	6.00	2.98E-11	3.00
9	2.91E-41	10.00	1.58E-32	8.00	2.15E-24	6.00	3.72E-12	3.00

polynomials $P_0^{r_k}$, $r_k = 9, 7, 5$, approximate x^3 perfectly. They also approximate the even $\cos(x)$ term to one better power, to $\mathcal{O}(h^{r_k+1})$, due to the fact that r_k is always odd in our tests and the grid is uniform. That is, these polynomials are of even degree and approximate an even function as well as a polynomial of one degree higher on a uniform grid. When the stencils avoid the discontinuity, we see superconvergence for these polynomials.

The new WENO-AO reconstructions will maintain accuracy when dropping order due to a discontinuity in the solution when $\eta_k \geq r_k/2$, according to (5.12) in Theorem 5.8. However, to see superconvergence, we need $\eta_k \geq (r_k + 1)/2$. Since we took the integral value $\eta_k = \lceil \frac{r_k}{2} \rceil = (r_k + 1)/2$, we had a large enough value to see superconvergence in the results shown in Tables 7.3–7.4, when $x_* \neq -h$. The latter case is limited by the base polynomial approximation to order 3. In fact, if we replace x^3 by x^2 in the solution $g(x)$, we recover superconvergent order 4 for this location of the discontinuity.

In Tables 7.3–7.4, the original WENO-AO$_3$ reconstructions show no superconvergence in the four cases that drop to the base level, i.e., they maintain order 3, as expected (moreover, they show order 4 if x^3 is replaced by x^2 in the solution $g(x)$). The largest stencil ($x_* = -4h$) also shows superconvergence for either weighting, since there is no discontinuity. When $x_* = -3h$, so the discontinuity is only on the largest stencil, WENO-JS weighting gives superconvergent order 6, but WENO-Z maintains order 7 rather than achieving superconvergent order 8. The reason is that we used $\eta_3 = 2$. Theorem 5.7 requires $\eta_3 \geq (6 - 3)/2 = 3/2$ to see superconvergence for

TABLE 7.5

Burger's equation. WENO-JS weights with $\epsilon_h = h^2$. Error and convergence rate on uniform grids at time $T = 0.25$.

	L^1		L^∞		L^1		L^∞	
N	Error	Order	Error	Order	Error	Order	Error	Order
	WENO-AO$_3(7,5,3)$				WENO-AO$(7,5,3)$			
40	3.90E-06	5.05	1.91E-05	4.45	1.92E-06	5.59	9.34E-06	5.01
80	1.09E-07	5.16	5.48E-07	5.12	2.21E-08	6.44	1.23E-07	6.24
160	3.24E-09	5.07	1.53E-08	5.16	1.95E-10	6.82	1.12E-09	6.78
320	9.95E-11	5.02	4.59E-10	5.06	1.57E-12	6.96	9.11E-12	6.95
	WENO-AO$_3(9,5,3)$				WENO-AO$(9,5,3)$			
40	2.50E-06	5.34	1.24E-05	4.69	4.78E-07	6.94	2.78E-06	6.11
80	9.41E-08	4.73	4.36E-07	4.83	1.82E-09	8.04	1.04E-08	8.06
160	3.11E-09	4.92	1.43E-08	4.93	4.96E-12	8.52	3.15E-11	8.37
320	9.85E-11	4.98	4.51E-10	4.99	5.75E-14	6.43	3.46E-13	6.50
	WENO-AO$_3(9,7,5,3)$				WENO-AO$(9,7,5,3)$			
40	2.50E-06	5.32	1.23E-05	4.65	5.14E-07	6.69	3.07E-06	5.74
80	9.41E-08	4.73	4.36E-07	4.82	2.40E-09	7.74	1.50E-08	7.68
160	3.11E-09	4.92	1.43E-08	4.93	6.06E-12	8.63	4.23E-11	8.46
320	9.85E-11	4.98	4.51E-10	4.99	1.41E-14	8.75	9.97E-14	8.73

TABLE 7.6

Burger's equation. WENO-Z weights with $\epsilon_h = h^2$. Error and convergence rate on uniform grids at time $T = 0.25$.

	L^1		L^∞		L^1		L^∞	
N	Error	Order	Error	Order	Error	Order	Error	Order
	WENO-AO$_3(7,5,3)$				WENO-AO$(7,5,3)$			
40	1.97E-06	5.52	9.66E-06	4.91	1.97E-06	5.52	9.65E-06	4.91
80	2.29E-08	6.43	1.29E-07	6.23	2.29E-08	6.43	1.29E-07	6.23
160	2.03E-10	6.82	1.18E-09	6.78	2.03E-10	6.82	1.18E-09	6.78
320	1.63E-12	6.96	9.53E-12	6.95	1.63E-12	6.96	9.53E-12	6.95
	WENO-AO$_3(9,5,3)$				WENO-AO$(9,5,3)$			
40	5.20E-07	6.60	3.12E-06	5.69	5.19E-07	6.50	3.11E-06	5.54
80	2.45E-09	7.73	1.53E-08	7.67	2.45E-09	7.73	1.53E-08	7.67
160	6.19E-12	8.63	4.34E-11	8.46	6.18E-12	8.63	4.33E-11	8.46
320	1.44E-14	8.75	1.02E-13	8.73	1.44E-14	8.75	1.02E-13	8.73
	WENO-AO$_3(9,7,5,3)$				WENO-AO$(9,7,5,3)$			
40	5.20E-07	6.59	3.12E-06	5.67	5.19E-07	6.49	3.11E-06	5.53
80	2.45E-09	7.73	1.53E-08	7.67	2.45E-09	7.73	1.53E-08	7.67
160	6.19E-12	8.63	4.34E-11	8.46	6.18E-12	8.63	4.33E-11	8.46
320	1.44E-14	8.75	1.02E-13	8.73	1.44E-14	8.75	1.02E-13	8.73

WENO-JS weights, but we need $\eta_2 \geq (8-3)/2 = 5/2 > 2$ for WENO-Z weights. Indeed, if we increase $\eta_3 = 3$, we see superconvergence order 8 for WENO-Z weights.

7.2. Burgers' equation. We next solve Burgers' equation $u_t + (u^2/2)_x = 0$ with the initial condition $u_0(x) = 0.25 + 0.5\sin(\pi x)$ on $[-1, 1]$ to the time $T = 0.25$. A shock forms in the solution after this time, but the solution sharpens up to time T so as to have a very steep front. The exact solution can be determined, and the convergence results are shown in Tables 7.5 and 7.6. We use the same parameters as in Example 7.1. Some of the computations use the long double data type to achieve the extreme accuracy reported.

Because Theorem 4.5 caps the order of accuracy at $2s-1 = 5$ when using WENO-JS weights, we see that the old WENO-AO$_3$ reconstruction is only fifth order accurate. It is nearly optimal using WENO-Z weights. The new WENO-AO reconstruction performs similarly using WENO-Z weights but improves the solution with WENO-JS weights. With these weights, we see nearly optimal results for WENO-AO$(7,5,3)$ and WENO-AO$(9,7,5,3)$, but WENO-AO$(9,5,3)$ seems to be only perhaps seventh order accurate. This is predicted by the condition (4.25) of Theorem 4.6, i.e., the maximum rate is capped at $5+3-1=7$.

7.3. The one-dimensional Euler system. The one-dimensional Euler system of gas dynamics is given by

$$\frac{\partial}{\partial t}\begin{pmatrix}\rho\\ m\\ E\end{pmatrix}+\frac{\partial}{\partial x}\begin{pmatrix}m\\ \rho u^2+p\\ u(E+p)\end{pmatrix}=0, \tag{7.1}$$

where $m=\rho u$, $E=p/(\gamma-1)+\rho u^2/2$ and ρ, u, m, p, and E are the density, velocity, momentum, pressure, and energy, respectively, and $\gamma=1.4$. We compare the two WENO-AO reconstructions on two of the more challenging standard test problems.

Following [2], let $\gamma_{\mathrm{Hi}}=\gamma_{\mathrm{Lo}}=0.85$. For WENO-AO$_3(7,5,3)$, take

$$\alpha_0^5=\gamma_{\mathrm{Hi}},\quad \alpha_{-1}^3=\alpha_1^3=(1-\gamma_{\mathrm{Hi}})(1-\gamma_{\mathrm{Lo}})/2,\quad \alpha_0^3=(1-\gamma_{\mathrm{Hi}})\gamma_{\mathrm{Lo}};$$
$$\gamma^{7,3}=\gamma_{\mathrm{Hi}},\quad \gamma^{5,3}=1-\gamma_{\mathrm{Hi}};$$
$$\eta_{0,1}=\eta_{0,2}=2,\quad \eta_2=1.$$

For WENO-AO$(7,5,3)$, take

$$\alpha_0^7=\alpha_0^5=\gamma_{\mathrm{Hi}},\quad \alpha_{-1}^3=\alpha_1^3=(1-\gamma_{\mathrm{Hi}})(1-\gamma_{\mathrm{Lo}})/2,\quad \alpha_0^3=(1-\gamma_{\mathrm{Hi}})\gamma_{\mathrm{Lo}};$$
$$\eta_1=2,\quad \eta_2=3.$$

For both reconstructions, we use $\epsilon=h^2$. We use the HLL numerical flux [7].

7.3.1. Shu and Osher's shock interaction with entropy waves. The shock interaction with entropy waves problem given in [15] has a moving Mach 3 shock interacting with sine waves in the density. The initial condition is

$$(\rho,u,p)=\begin{cases}\rho_l=3.857143,\ u_l=2.629396,\ p_l=10.333333, & \text{for } 0<x<0.1,\\ \rho_r=1+0.2\sin(5(10x-5)),\ u_r=0,\ p_r=1, & \text{for } 0.1<x<1.\end{cases}$$

We compute the density at $T=0.16$ using $\Delta t=0.1\Delta x$ and $N=400$ cells. The results are shown in Figure 7.1. We see little difference between the two reconstructions, although perhaps the new one reaches the peaks of the sine waves slightly better.

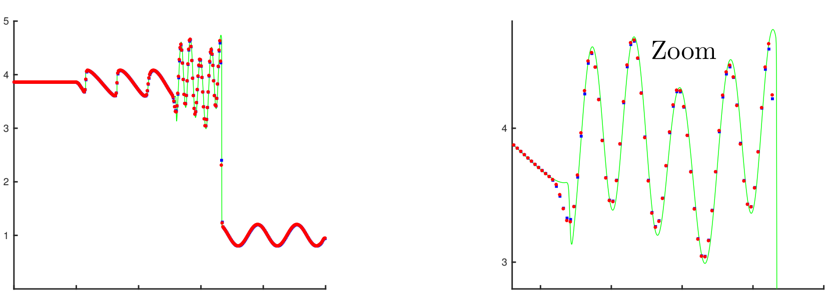

FIG. 7.1. *Shu and Osher's shock interaction. The density at $T=0.16$ using $N=400$ cells. The plots are the reference solution (green line), WENO-AO$_3(7,5,3)$ (blue squares), and WENO-AO$(7,5,3)$ (red circles) with WENO-Z weights.*

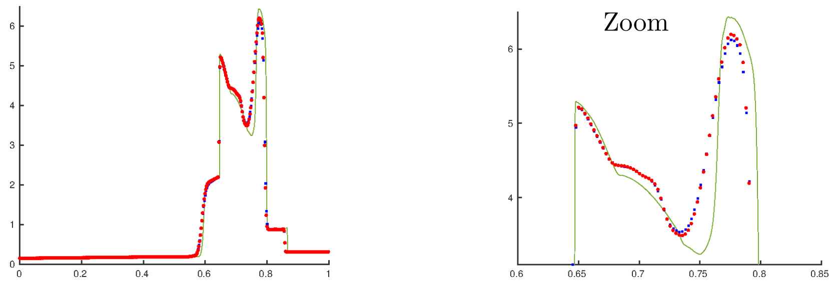

FIG. 7.2. *Woodward and Colella's double blast test. The density at $T = 0.038$ using $N = 399$ cells. The plots are the reference solution (green line), WENO-AO$_3(7,5,3)$ (blue squares), and WENO-AO$(7,5,3)$ (red circles) with WENO-Z weights.*

7.3.2. Woodward and Colella's double blast test. The last test uses the initial condition

$$(\rho, m, E) = \begin{cases} \rho_l = 1,\ m_l = 0,\ E_l = 1000/(\gamma - 1), & \text{for } 0 < x < 0.1, \\ \rho_m = 1,\ m_m = 0,\ E_m = 0.01/(\gamma - 1), & \text{for } 0.1 < x < 0.9, \\ \rho_r = 1,\ m_r = 0,\ E_r = 100/(\gamma - 1), & \text{for } 0.9 < x < 1. \end{cases}$$

Two shock waves form and interact before time $T = 0.038$, so this is a particularly challenging example. The density at time $T = 0.038$ is shown in Figure 7.2. The new reconstruction captures the solution a bit better.

REFERENCES

[1] F. Aràndiga, A. Baeza, A. M. Belda, and P. Mulet, *Analysis of WENO schemes for full and global accuracy*, SIAM J. Numer. Anal., 49 (2011), pp. 893–915.

[2] D. S. Balsara, S. Garain, and C.-W. Shu, *An efficient class of WENO schemes with adaptive order*, J. Comput. Phys., 326 (2016), pp. 780–804.

[3] R. Borges, M. Carmona, B. Costa, and W. Don, *An improved weighted essentially non-oscillatory scheme for hyperbolic conservation laws*, J. Comput. Phys., 227 (2008), pp. 3191–3211.

[4] M. Castro, B. Costa, and W. Don, *High order weighted essentially non-oscillatory WENO-Z schemes for hyperbolic conservation laws*, J. Comput. Phys., 230 (2011), pp. 1766–1792.

[5] I. Cravero, G. Puppo, M. Semplice, and G. Visconti, *CWENO: Uniformly accurate reconstructions for balance laws*, Math. Comp., 87 (2018), pp. 1689–1719.

[6] W.-S. Don and R. Borges, *Accuracy of the weighted essentially non-oscillatory conservative finite difference schemes*, J. Comput. Phys., 250 (2013), pp. 347–372.

[7] A. Harten, P. D. Lax, and B. van Leer, *On upstream differencing and Godunov-type schemes for hyperbolic conservation laws*, SIAM Rev., 25 (1983), pp. 35–61.

[8] A. Harten and S. Osher, *Uniformly high-order accurate nonoscillatory schemes* I, SIAM J. Numer. Anal., 24 (1987), pp. 279–309.

[9] A. K. Henrick, T. D. Aslam, and J. M. Powers, *Mapped weighted essentially non-oscillatory schemes: Achieving optimal order near critical points*, J. Comput. Phys., 207 (2005), pp. 542–567.

[10] G.-S. Jiang and C.-W. Shu, *Efficient implementation of weighted ENO schemes*, J. Comput. Phys., 126 (1996), pp. 202–228.

[11] O. Kolb, *On the full and global accuracy of a compact third order WENO scheme*, SIAM J. Numer. Anal., 52 (2014), pp. 2335–2355.

[12] D. Levy, G. Puppo, and G. Russo, *Compact central WENO schemes for multidimensional conservation laws*, SIAM J. Sci. Comput., 22 (2000), pp. 656–672.

[13] X. D. Liu, S. Osher, and T. Chan, *Weighted essentially non-oscillatory schemes*, J. Comput. Phys., 115 (1994), pp. 200–212.

[14] C.-W. Shu and S. Osher, *Efficient implementation of essentially non-oscillatory shock capturing schemes*, J. Comput. Phys., 77 (1988), pp. 439–471.
[15] C.-W. Shu and S. Osher, *Efficient implementation of essentially non-oscillatory shock capturing schemes* II, J. Comput. Phys., 83 (1989), pp. 32–78.
[16] J. Zhu and J. Qiu, *A new fifth order finite difference WENO scheme for solving hyperbolic conservation laws*, J. Comput. Phys., 318 (2016), pp. 110–121.